Report No. ACNP 62012

PATHFINDER ATOMIC POWER PLANT
TECHNICAL PROGRESS REPORT

JANUARY 1962 – MARCH 1962

Submitted to

U. S. ATOMIC ENERGY COMMISSION

NORTHERN STATES POWER COMPANY

and

CENTRAL UTILITIES ATOMIC POWER ASSOCIATES

by

ALLIS-CHALMERS MANUFACTURING COMPANY
ATOMIC ENERGY DIVISION
Milwaukee 1, Wisconsin

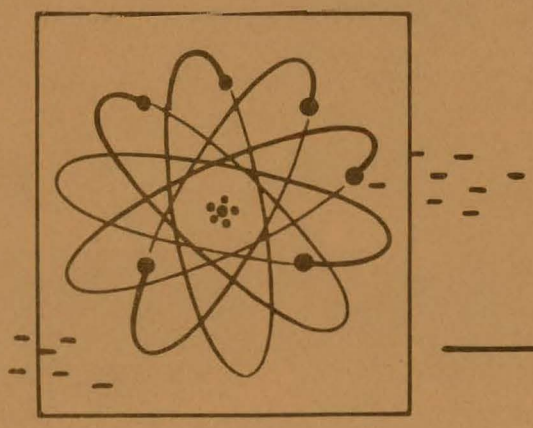

Ref: AEC Contract No. AT(11-1)-589

DISCLAIMER

LEGAL NOTICE

PATHFINDER ATOMIC POWER PLANT
TECHNICAL PROGRESS REPORT

JANUARY 1962 – MARCH 1962

Submitted to

U. S. ATOMIC ENERGY COMMISSION
NORTHERN STATES POWER COMPANY
and
CENTRAL UTILITIES ATOMIC POWER ASSOCIATES

by

ALLIS-CHALMERS MANUFACTURING COMPANY

Under
Agreement dated 2nd Day of May 1957, as Amended
between
Allis-Chalmers Mfg. Co. & Northern States Power Co.
under
AEC Contract No. AT(11-1)-589

June 30, 1962

Classification – UNCLASSIFIED

Reviewed by R W Klecker
Authorized Classifying Official

Approved: C. B. Graham
C. B. Graham
Manager
Nuclear Power Dept.-Greendale

ALLIS-CHALMERS MANUFACTURING COMPANY
ATOMIC ENERGY DIVISION
MILWAUKEE 1, WISCONSIN

Approved: Hibbert Hill
Hibbert Hill
Chief Engineer

NORTHERN STATES POWER COMPANY
15 SOUTH FIFTH STREET
MINNEAPOLIS 2, MINNESOTA

ACNP-62012

PATHFINDER ATOMIC POWER PLANT
TECHNICAL PROGRESS REPORT
JANUARY 1962 - MARCH 1962

DISTRIBUTION

USAEC, Chicago Operations Office - 9800 South Cass Avenue, Argonne, Illinois		8
USAEC, Division of Reactor Development - Washington 25, D. C.		8
USAEC, OTIE - Oak Ridge, Tennessee	OFFSET MASTERS PLUS	20
Northern States Power Company		35
Allis-Chalmers Manufacturing Company		39
	TOTAL	110

THIS PAGE

WAS INTENTIONALLY

LEFT BLANK

CONTENTS

FIGURES

FIGURES (Continued)

FIGURES (Continued)

FOREWORD

This is one of a series of reports covering technical progress on the research and development program being performed in connection with the design of the Pathfinder Atomic Power Plant. This plant will be located at a site near Sioux Falls, South Dakota and is scheduled for operation in late 1962. Owners and operators of the plant will be the Northern States Power Company of Minneapolis, Minnesota.

The U. S. Atomic Energy Commission, through Contract No. AT(11-1)-589, with Northern States Power Company, and Central Utilities Atomic Power Associates* (CUAPA), are sponsors of the research and development program.

Allis-Chalmers Manufacturing Company of Milwaukee, Wisconsin, under contract with Northern States Power Company, is performing the research, development, and design; and will construct the plant including the reactor, which is designated the Controlled Recirculation Boiling Reactor (CRBR) with Nuclear Superheater. Pioneer Service and Engineering Company of Chicago, Illinois is providing the architect-engineer services to Allis-Chalmers. Portions of the R & D program, particularly in connection with fuel development, have been subcontracted by Allis-Chalmers.

---

*CUAPA MEMBER COMPANIES:

Central Electric and Gas Company
Interstate Power Company
Iowa Power and Light Company
Iowa Southern Utilities Company
Madison Gas and Electric Company
Northern States Power Company
Northwestern Public Service Co.
Otter-Tail Power Company
St. Joseph Light and Power Co.
Wisconsin Public Service Corp.

DESIGN DATA

CRBR WITH NUCLEAR SUPERHEATER

Plant

Power, boiler region	157,200 kw
Power, superheater region	42,400 kw
Steam flow at rated power	616,125 lbs/hr
Total core power	199,600 kw
Gross electrical capability	66,000 kw
Net electrical output	62,000 kw
Net efficiency	31.0 per cent
Steam outlet pressure (reactor)	535 psig
Reactor operating pressure	600 psig
Temperature, boiler region	489 F
Outlet temperature, superheater region	825 F
Gross heat rate	10,199 Btu/kw-hr
Reactor building size	50 ft dia x 120 ft

Reactor

Vessel size (overall)	11 ft 6 in o.d. 36 ft 1 in
Total core dimensions	6 ft x 6 ft
Dimensions of superheater region	6 ft x 30 in
Fuel, boiler (Zr-2 clad)	approx. 2.2 per cent enriched UO_2
Fuel, superheater (S.S. clad)	approx. 93 per cent enriched UO_2
Fuel, loading, boiler (U-235)	145.6 kg
Fuel, loading, superheater (U-235)	42 kg
Power density (boiler core coolant)	87 kw/liter
Average heat flux, boiler region	128,000 Btu/hr-ft^2
Average heat flux, superheater region	77,800 Btu/hr-ft^2
Maximum heat flux, boiler region	462,000 Btu/hr-ft^2
Maximum heat flux, superheater region	245,000 Btu/hr-ft^2
Recirculation rate	65,000 gpm
Recirculation pump power	823 kw
Neutron flux	approx. 5×10^{15} n/cm^2-sec

1. FUEL ELEMENT RESEARCH AND DEVELOPMENT

THIS PAGE

WAS INTENTIONALLY

LEFT BLANK

1.1 FUEL MATERIAL CLADDING, BONDING, AND IRRADIATION TESTING

The objectives of this project are as follows: 1) to perform laboratory work on the material and thermal properties of boiler fuel elements in the following two general areas: (a) fuel cladding testing and investigations, as required, and (b) complete aluminum capsule irradiation proof-testing together with pre- and post-irradiation examinations; 2) to develop a high-enrichment uranium-dioxide-stainless-steel-cermet fuel element clad with stainless steel or a suitable alternate material, which includes development of means of maintaining alignment and spacing of fuel bearing tubes and double-walled insulating tubes, development of conceptual designs for the steam entry and exit section supporting the element, evaluation of assembly techniques, and fabrication of a steam corrosion-erosion test loop and testing of superheater fuel cladding material; and 3) to develop means of inserting burnable poison in the reactor core, as required, and to perform studies and research and development on in-core instrumentation for the boiler region flux and coolant flow distribution and for superheater region temperature, flux, and coolant flow.

1.1.1 STEAM CORROSION-EROSION TESTS ON STAINLESS STEELS

The second phase of the erosion-corrosion test, a 3-month test of 304, 304L, 316, and 316L stainless steels under simulated reactor conditions, is in process. As described in ACNP-6123, test conditions in the superheated-steam test section are as follows: 700 F, 670 psig, 2400 lb/hr, and 250 fps. Conditions in the saturated-steam test section are: 489 F, 600 psig, 99.5 to 99.9 per cent quality, 2400 lb/hr, 175 fps, and 30 ppm oxygen concentration. Periodic blowdown of the test loop is used to maintain high-purity water conditions.

The test schedule calls for removal of 304L and 316L samples with replacement by 304 and 316 samples at 3-week intervals. This procedure has made possible a preliminary determination of the corrosion rate of 304L and 316L. Similar information for 304 and 316 will be obtained at the conclusion of the test when all remaining samples will be examined, weighed, descaled, reweighed, and re-examined.

Preliminary test results indicate that corrosion of samples in the saturated-steam section is greater than in the superheated-steam section.

Furthermore, surface penetration of 316L stainless steel in the saturated-steam section is significantly greater than penetration of 304L. However, the projected corrosion rate, assuming a pessimistic linear dependency, remains less than the 0.1 mil per year for stainless steels under these conditions. No characteristic streaking or erosive pitting has been detected on any samples removed to date.

Tabulations of test results for three 3-week periods are given in Tables 1.1 and 1.2. Surface penetration in mils (Table 1.1) is based on the difference between sample weight after and before exposure.

TABLE 1.1 SURFACE PENETRATION OF STAINLESS STEEL IN SATURATED AND SUPERHEATED STEAM

MATERIAL	PERIOD (3 wk)	SURFACE PENETRATION	
		SUPERHEATED STEAM (mils)	SATURATED STEAM (mils)
304L	1	.001	.002
	2	.0025	.0035
	3	.0025	.005
316L	1	<.001	.007
	2	.001	.009
	3	.003	.015

TABLE 1.2 WEIGHT GAIN OF STAINLESS STEEL SAMPLES IN SUPERHEATED AND SATURATED STEAM

MATERIAL	PERIOD (3 wk)	WEIGHT GAIN	
		SUPERHEATED STEAM (md)	SATURATED STEAM (md)
304L	1	8	10
	2	8	12
	3	10	15
316L	1	-	22
	2	5	26
	3	10	40

I.2 HEAT TRANSFER AND FLUID FLOW INVESTIGATIONS

Objectives of this project are to operate an experimental apparatus (heat transfer loop) to measure heat transfer coefficients and two-phase pressure drops for a full-sized coolant channel. Installed power capacity of the test loop shall be such that it will allow testing of 1) one fuel coolant channel at a heat flux of one million Btu/hr-ft^2 or 2) one-half of a fuel channel at a heat flux of two million Btu/hr-ft^2. The maximum design pressure and temperature shall be 1500 psi and 596 F.

Tests will be performed to determine 1) dimensional stability of fuel elements by thermal cycling, 2) pressure drop and vibration tendencies at various flow rates, 3) heat transfer coefficients under simulated Pathfinder operating conditions, and 4) the ability of a superheater element to cool itself by radiation and convection under conditions equivalent to fission product heating with no forced steam flow and with no steam flow.

I.2.1 HEAT TRANSFER LOOP

Construction of an addition to the laboratory requires that the steam condenser and cooling-water heat exchanger of the heat transfer loop be moved to the laboratory roof. This change with associated changes in piping will require about one month.

I.2.2 BOILER FUEL ELEMENTS

I.2.2.1 16-Pin Void Distribution. Gamma attenuation measurements on a 4 x 4 rod array were made to determine the void distribution at simulated reactor conditions. Test conditions were nominally:

pressure	615 psia
mass velocity	1 x 10^6 to 2 x 10^6 lb/hr-ft^2
heat flux	50,000 to 150,000 Btu/hr-ft^2
steam quality	0.005 to 0.032

The test was conducted and data were reduced by methods used for earlier air-water and lucite-model tests, which indicated an experimental error no more than 5 percent absolute void fraction.

Five sets of traverses were completed. Two sets were carried out immediately above a spacer in the lower half of the test section at mass velocities of 2.18 x 10^6 and 1.23 x 10^6 lb/hr-ft^2 with steam qualities of 0.0053 and

0.0082, respectively. Three sets were carried out immediately below a spacer in the upper half at mass velocities of 1.92×10^6, 1.06×10^6, and 1.08×10^6 with steam qualities of 0.0163, 0.0208, and 0.0354, respectively. The manner in which the runs were made is indicated in Figure I.I.

Each set included four 100-point horizontal traverses as follows: 1) with the test section empty at zero power; 2) with the test section full of saturated water at 489 F, 615 psia at zero power; 3) with the section full of water at 489 F, 700 psia at the test power; and 4) with the test section containing the two-phase mixture at 489 F, 615 psia at the test power. Traverses 1 and 2 were made to calibrate the empty and water-filled test section at zero power. Traverse 3 was made to calibrate a liquid filled section at test power. The latter calibration traverse was necessary since a comparison of count rates for traverses 2 (zero power) and 3 (test power) had shown small differences, which were attributable to the effect of the magnetic field on the shielded photomultiplier tube during traverses at power. The difference in count rates never exceeded 3 per cent.

The count rates were plotted versus horizontal position, and the data were adjusted horizontally to compensate for movement of loop piping between successive traverses. (The gamma equipment could be positioned exactly). The largest shift for the five sets of traverses was 0.060 in.

Local void fractions were computed for each horizontal position. These local void fractions were plotted as a function of horizontal displacement from the center line of the nearest row of pins, which resulted in eight separate regions, as shown in Figure I.I. The data for a typical run are shown in Figures I.2, I.3, and I.4. Data representing the four central regions of the bundle are superposed in Figure I.2. Figure I.3 shows the

data representing the two regions just inside the outer rows of pins. Figure I.4 shows the data representing the two regions adjacent to the inner walls of the box. The curves show mean values for the data. Figure I.5 shows the data for a complete traverse without superposition of regions.

The data shown in Figure I.5 are typical of all runs with respect to the general shape of the mean void distribution. Figure I.5 indicates a slight tendency of the voids to be highest at the center of the complete traverse. The data clearly indicate that the void fraction goes to zero at the inner unheated walls of the enclosure. The data also indicate the higher void fractions in the regions between the pins, which agrees with the results reported earlier for an unheated, air-water system.

Each point in Figure I.5 represents a mean value for void fraction through the test section on the gamma path. An explanation of the physical significance of the shape taken by these values when plotted as a function of horizontal position would require parallel analytical studies. Various void distributions would be postulated for a horizontal cross section of the test section in attempts to find a distribution that would yield mean values of the same relative magnitudes as those obtained in the test.

The overall integrated void fractions for the five runs are shown in Figure I.6 compared to existing models and correlations. Also shown are two points for the 81-pin test section.

The data appear to exhibit appreciable scatter; however, in light of the complicated nature of the distributions within the bundle, this is difficult to assess. Moreover, an error of 1 F in measuring the inlet temperature is possible, which would result in an error in the quality measurement of 0.0016.

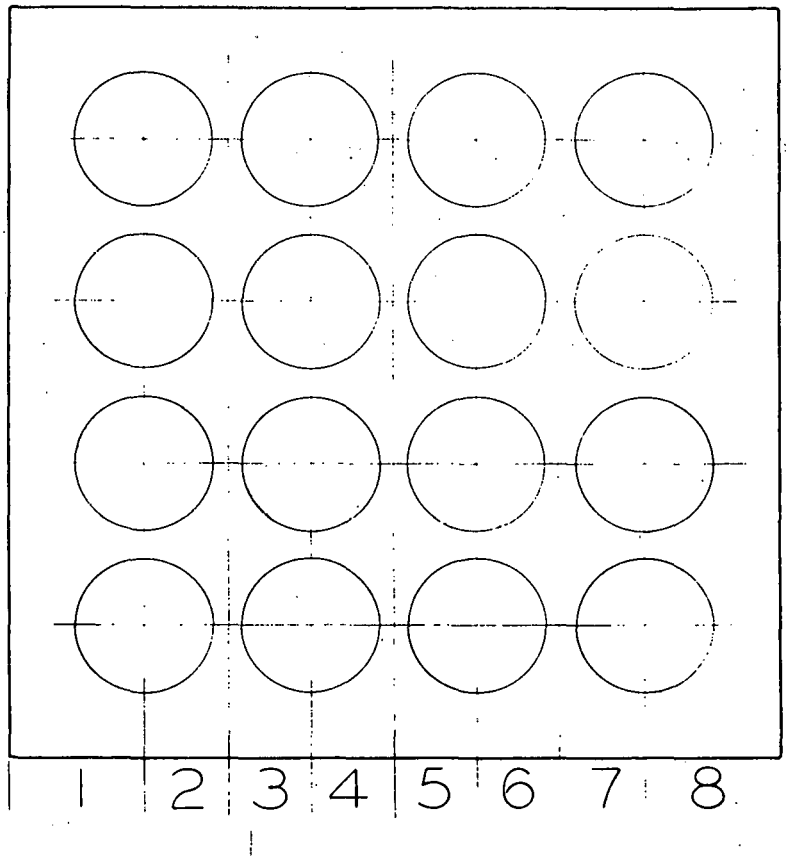

LOWER HALF
$\bar{R}_g = 0.278$
$X = 0.0082$
$G = 1.23 \times 10^6$
$\Phi = 158{,}500$

Figure 1.1 Cross section of 16-pin test section. Data was taken at 100 points over the eight indicated regions. (A-C Dwg 43-025-134)

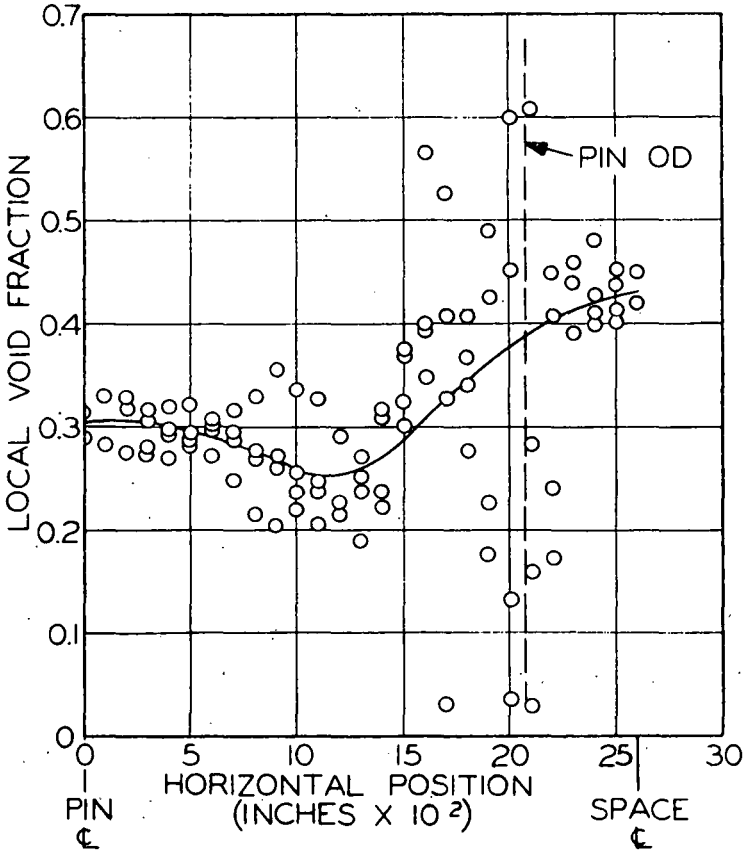

Figure 1.2 Typical local void fraction data for 16-pin test section. Data for regions 3, 4, 5, and 6 are superposed. Test conditions: lower half; $\bar{R}g=0.278$; $X=0.0082$; $G=1.23X10$; $\varphi=158,500$. (A-C Dwg 43-025-027)

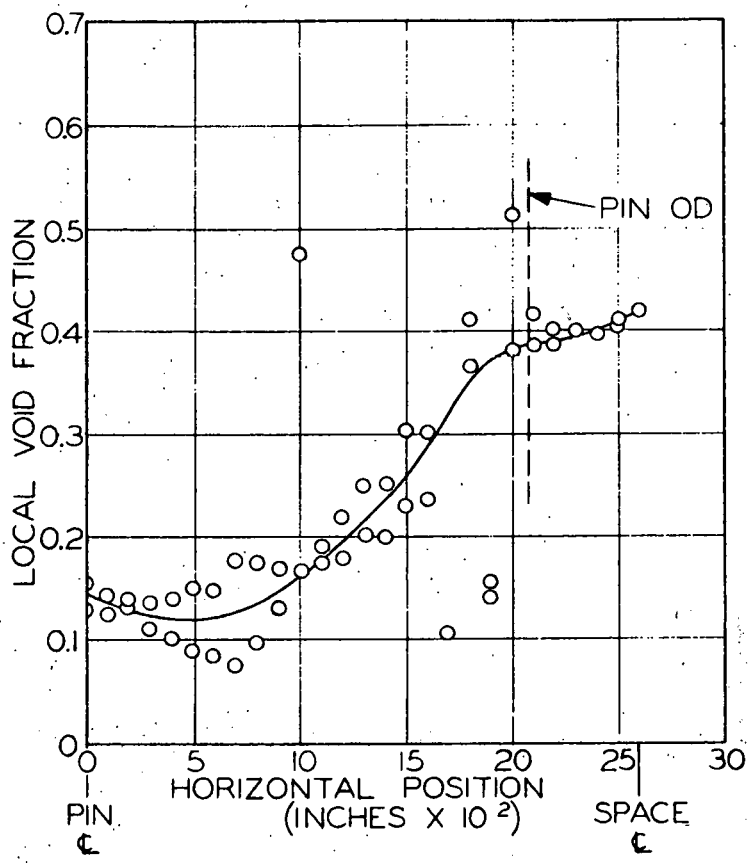

Figure 1.3 Typical local void fraction for 16-pin test section. Data for regions 2 and 7 are superposed. Test conditions are as given in Figure 1.2.
(A-C Dwg 43-025-028)

Figure 1.4 Typical local void fraction data for 16-pin test section. Data for regions 1 and 8 are superposed. Test conditions are as given in Figure 1.2.
(A-C Dwg 43-025-029

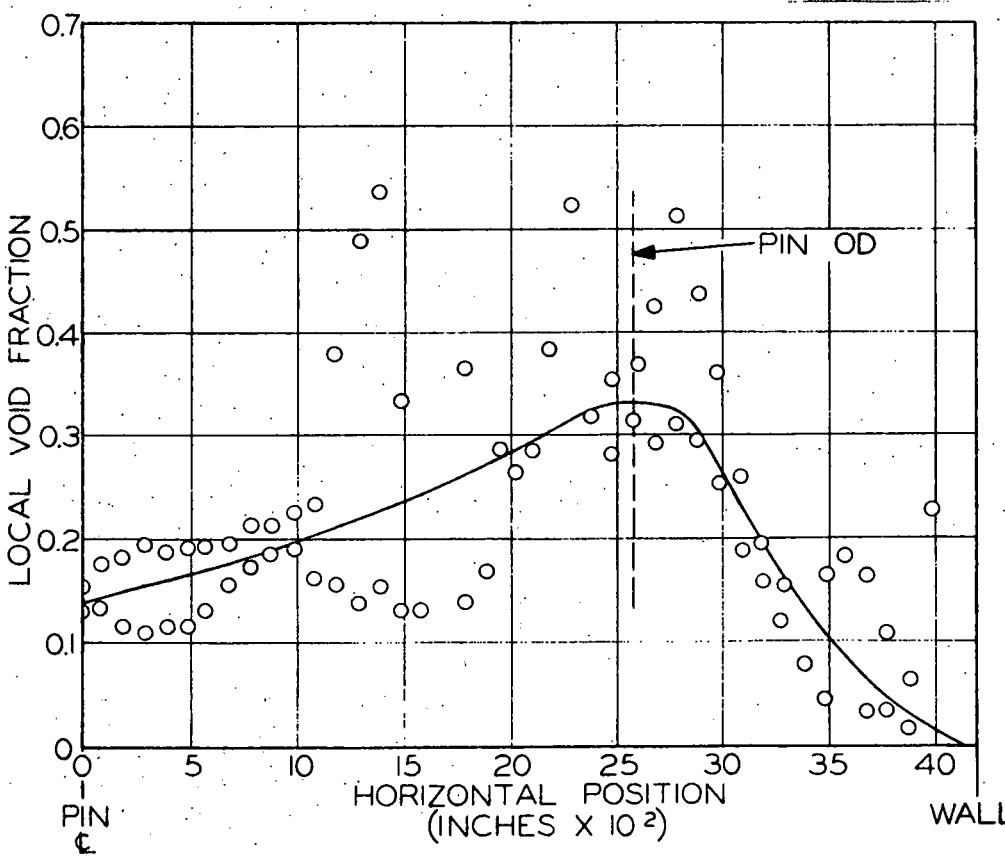

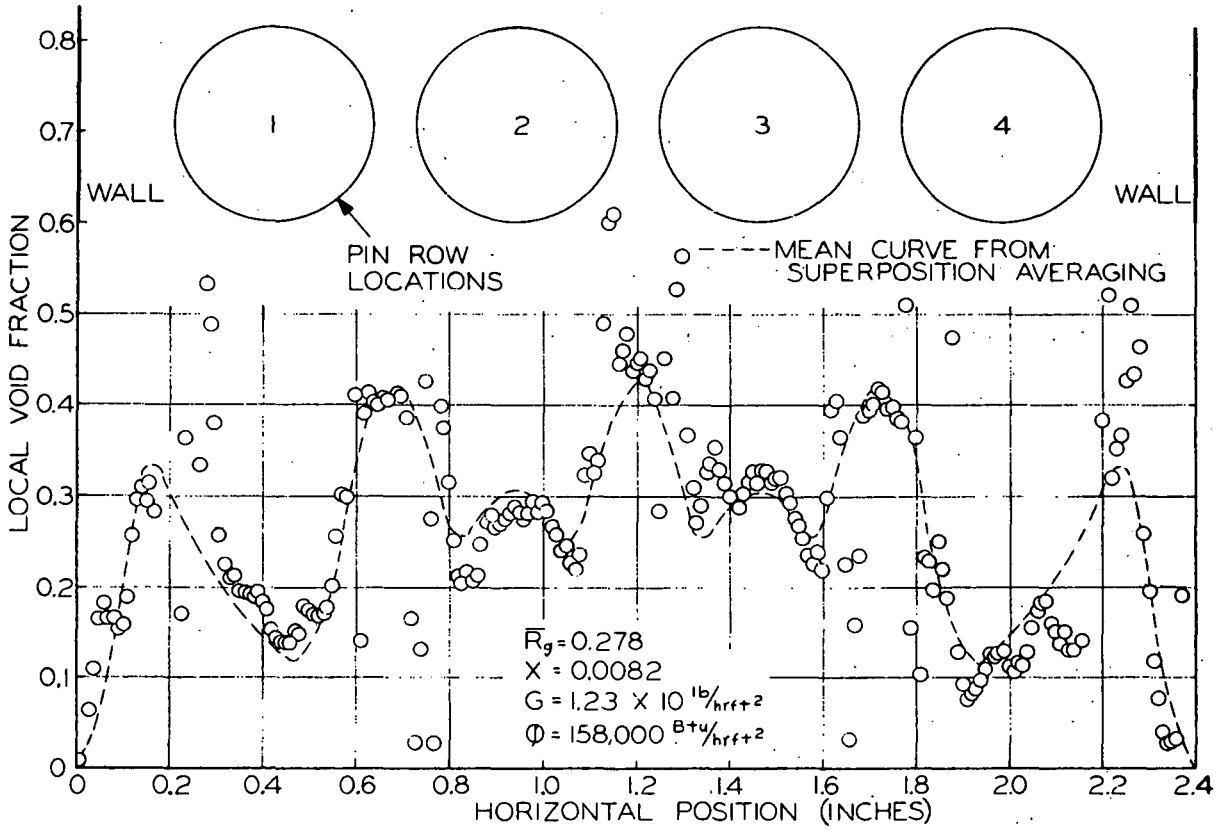

Figure 1.5 Typical local void fraction data. Data is plotted with no superposition of regions. The dotted curve represents the mean of superposed data. Test conditions are as given in Figure 1.2. (A-C Dwg 43-025 021)

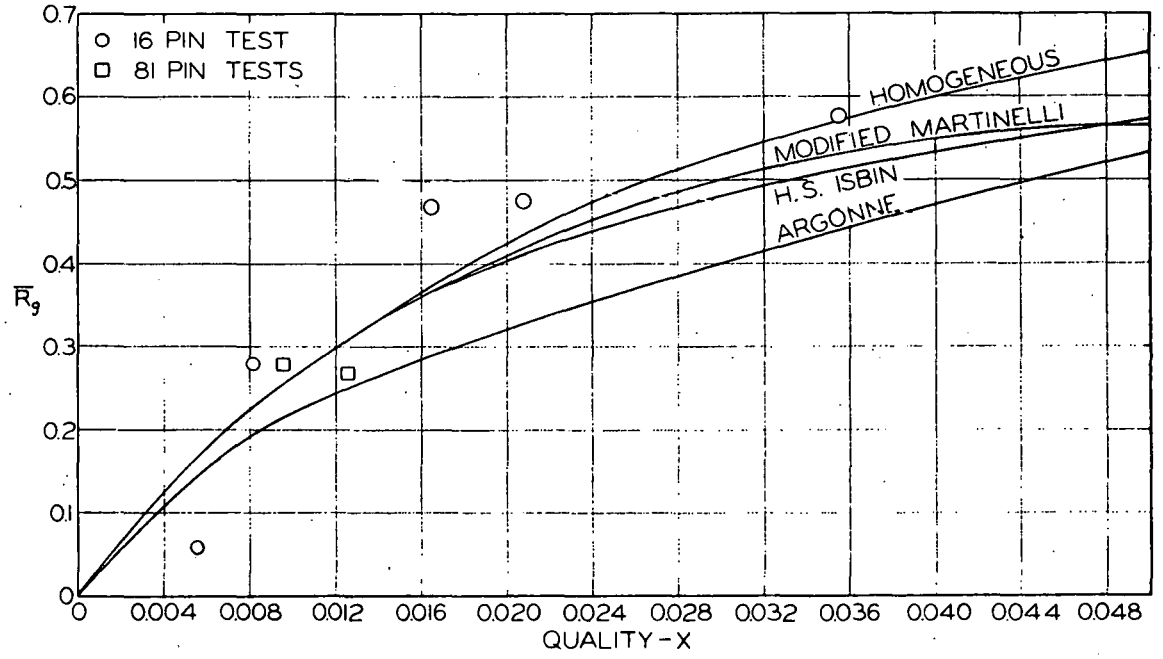

Figure 1.6 Overall mean steam-water void fraction (R_g) at 600 psia. Source of the "Argonne" curve is Figure III-19, ANL 6063 with G = 2 x 10^6 lb/hr-ft^2. (A-C Dwg 43-025-023)

It is felt that the data in Figure 1.5 tends to support the homogeneous model more than any of the other three relations. The homogeneous model gives void fractions slightly higher than the modified-Martinelli correlation used in the Pathfinder pressure-drop design calculations. However, this difference is well within the uncertainty limits assumed in making the calculations.

The entire pressure-drop and void test program for the boiler fuel element has now been completed, and the results will be presented in a forthcoming topical report.

1.2.3 SUPERHEATER FUEL ELEMENT

1.2.3.1 Superheater Heat Transfer Tests. Heat transfer and pressure drop tests have been completed on two test sections that simulate the center channel of the Pathfinder high-enrichment superheater fuel element. The heated test section provided an annular channel of 0.997 in. o.d. and 0.878 in. o.d.. The section was heated by electrical resistance heating in both walls.

In addition to the heated section, an isothermal test section of the same dimensions was installed downstream of the heated section. This section was tested simultaneously to determine pressure drop.

The range of test conditions were:

steam temperature	489 to 1220 F
mass flow rates	0.13×10^6 to 0.72×10^6 lb/hr-ft^2
surface heat flux	up to 125,000 Btu/hr-ft^2

The test data were reduced to conventional heat transfer and pressure drop dimensionless parameters. The heat transfer data were in good agreement ($\pm$ 15 percent) with the correlation of Heineman (ANL-6213). Friction factors for both the heated and isothermal test sections were accurately described ($\pm$ 10 percent) by the smooth Moody curve if fluid properties are evaluated

at the film temperatures. These data, in dimensionless form, are compared with their respective correlations in Figures 1.7, 1.8, and 1.9. Also shown in Figure 1.7 is the Pathfinder design equation for a film temperature of 800 F reduced by the 1.1 hot-spot factor. Comparison with data shows that the design relation is satisfactory without modification.

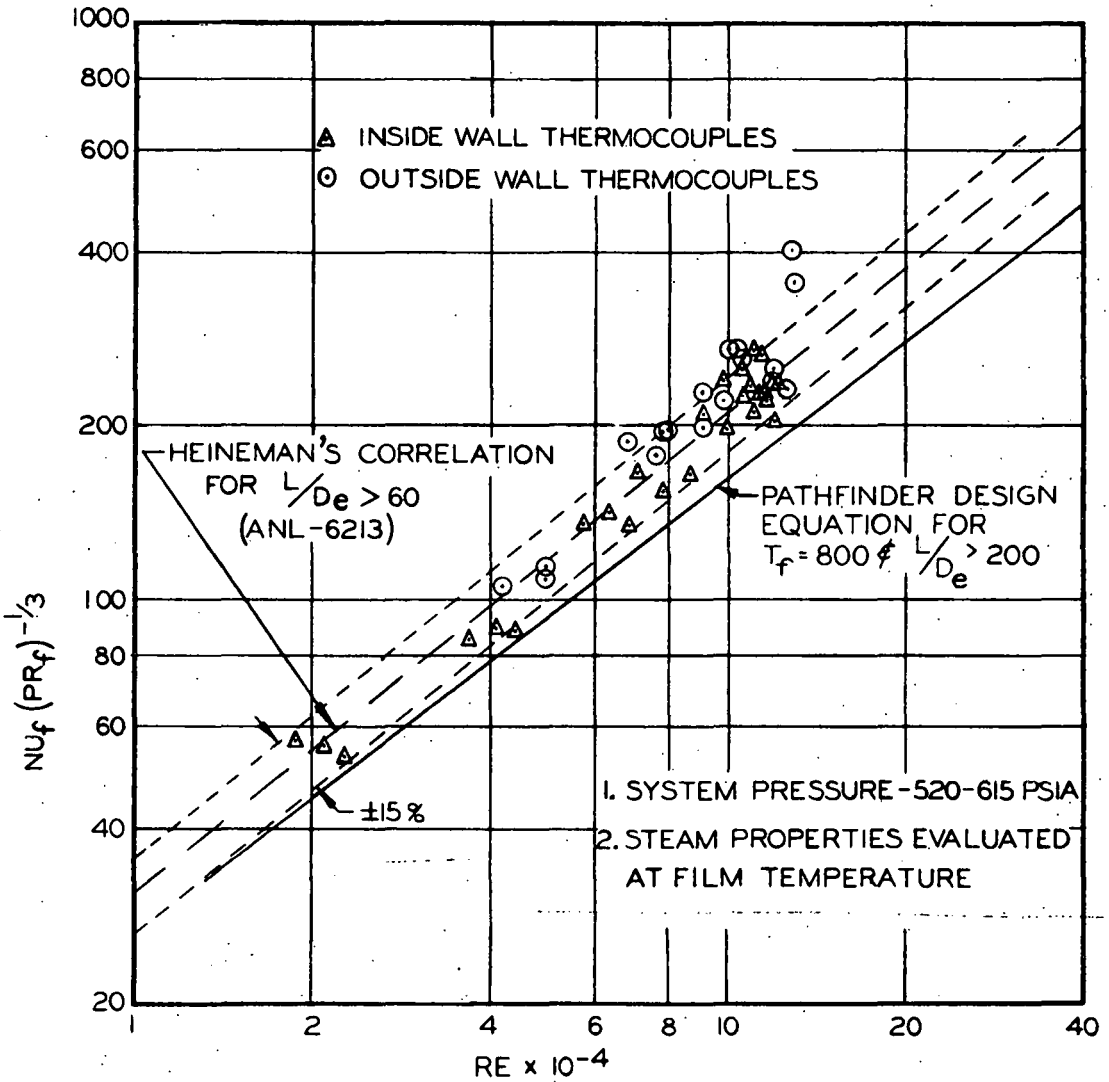

Figure 1.7 Heat transfer coefficients for a simulated Pathfinder superheater center flow channel. (A-C Dwg 43-024-974)

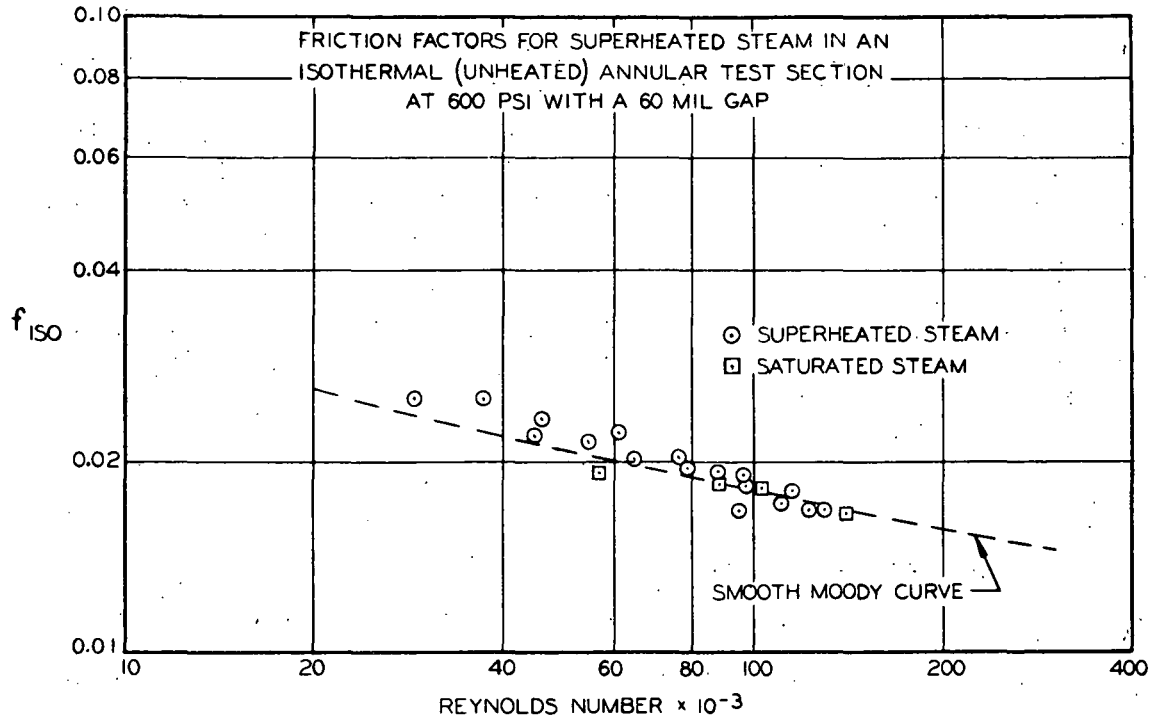

Figure 1.8 Friction factors for superheated steam in an isothermal (unheated) annular test section at 600 psi with a 60-mil gap. (A-C Dwg 43-024-975)

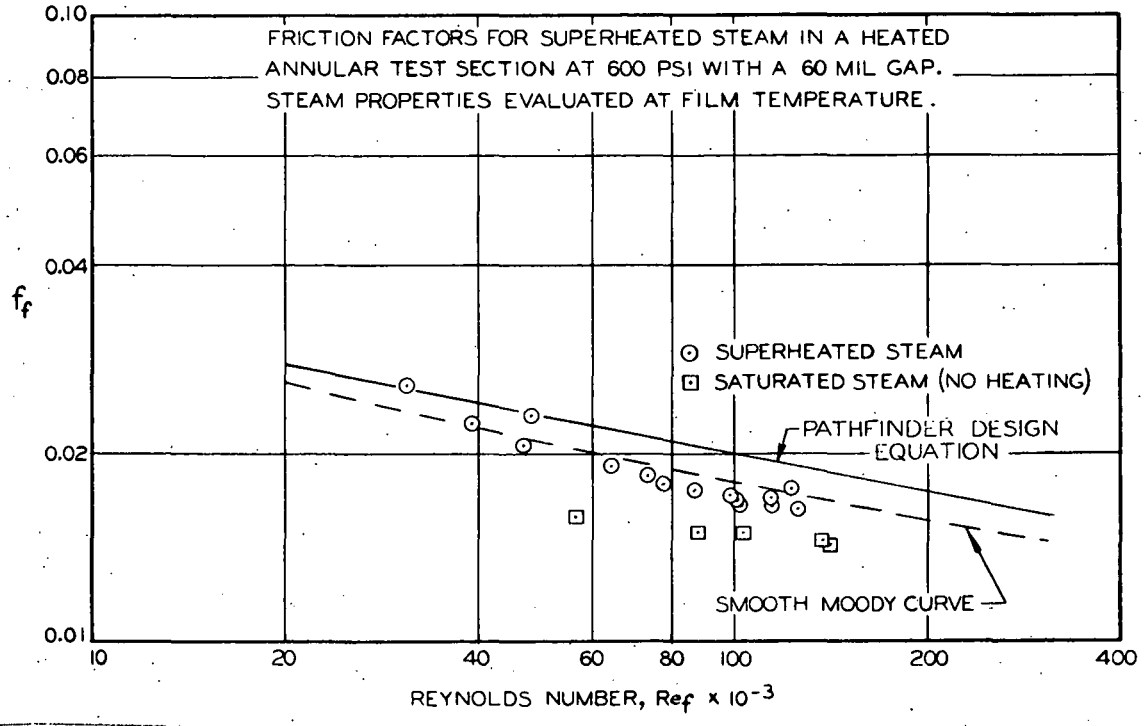

Figure 1.9 Friction factors for superheated steam in a heated annular test section at 600 psi with a 60-mil gap. Steam properties evaluated at film temperature. (A-C Dwg 43-024-976)

1.4 FUEL ELEMENT MANUFACTURING RESEARCH AND DEVELOPMENT

Objectives of this project are: 1) to develop or specify methods for production of fuel assemblies for the reactor core; and 2) to fabricate and examine sample boiler and high-enrichment superheater fuel assemblies (or portions thereof) to evaluate their suitability for repetitive fabrication to design specifications.

Development will include fuel fabrication, clad fabrication, fuel loading and sealing, assembly weldments, and intermediate and final inspection procedures, as required.

1.4.1 HIGH-ENRICHMENT SUPERHEATER FUEL ELEMENT

1.4.1.1 Fabrication and Assembly. As reported in the last quarterly progress report, the development of a hot rolling process for producing fuel tubes was completed. As previously reported, the greatest noticeable difference with isostatic pressing was an increase in density of approximately 1 per cent. This further supports the conclusion that the hot rolling process is satisfactory for producing the Pathfinder superheater fuel elements.

Work has been continuing on the development of full-length fuel element assemblies using the hot rolling process. Natural uranium dioxide has been processed through the production powder facilities, and the powder was further processed into ten large and ten small diameter fuel tubes. These tubes will be used for spacer wire welding, assembly and inspection studies, and development of fabrication techniques. Excessive powder losses were encountered at the startup of the production spraying operation. This was corrected by adding two absorption towers plus an additional absolute filter to the system.

The powder rolling mill was rebuilt to produce a full-width powder rolled strip that can be hot rolled into satisfactory cermet strip.

Both annealed and 1/4 hard stainless steel tubing for cladding were evaluated for draw-bonding characteristics. The 1/4 hard stainless steel tubing will be used for the production of fuel elements.

The homogeneity within a powder rolled batch and between the powder rolled strip and offal material is being evaluated.

The alumina-boron carbide poison pellet specification was completed and a vendor was selected.

GE 81 brazing alloy for use in brazing the guide fin assemblies was studied, and was found to be satisfactory.

1.6 DEVELOPMENT OF LOW-ENRICHMENT SUPERHEATER FUEL ELEMENTS

The objectives of this project are to determine the economic merit of using low-enrichment superheater fuel, to determine and select a promising fuel element design, and to develop a low-enrichment superheater fuel element through applicable studies, fabrication experiments, and testing.

At such a time as a promising fuel element concept has been selected, a full-scale mock-up will be fabricated including supports and steam entry and exit section, and flow tests will be performed to determine pressure drop and dimensional stability at simulated reactor operating conditions.

Heat transfer calculations will be performed. A test element will be fabricated for insertion in the heat transfer loop to perform heat transfer experiments under simulated Pathfinder operating conditions. Physics calculations will be performed, such as the required computer programming and operation, determination of the critical mass, neutron and gamma flux and power distribution, enrichment, coefficients of reactivity, control rod effectiveness, and conversion ratio.

A partial loading of prototype low-enrichment elements will be fabricated and tested in the critical facility in conjunction with the remainder of the superheater section of the core containing high-enrichment fuel elements. Safeguards reports will be prepared for the facility as required to meet the licensing requirements of the AEC. Critical experiments will be conducted to determine the nuclear characteristics of the prototype low-enrichment superheater fuel elements.

1.6.1 NUCLEAR DESIGN

1.6.1.1 Superheater Power Distribution with Depletion. Section 1.6.1 of ACNP-62005 described results from a PDQ-RZ depletion study of a low-enrichment superheater core. For this study, the superheater fuel element was assumed to be a cluster of seven 0.235-in o.d. uranium dioxide fuel rods of 4.5-a/o U-235 enrichment. The burnable poison, B-10, was homogeneously distributed in the center fuel pin of the cluster.

During the quarter, more detailed studies were made of power peaking with depletion caused by the superheater control-rod channels and the corners of the superheater-boiler interface. The calculations were performed as follows.

Two-dimensional XY calculations were performed for radial slices through

the upper and lower regions of the beginning-of-life core. The resulting power distributions were synthesized with comparable RZ calculations using techniques described in ACNP-6123. Results indicated that the superheater peak power is in the upper core region. The RZ depletion studies had indicated that the superheater power distribution remains quite stable with core life assuming the superheater control rods remain fully withdrawn during core life. Thus, XY depletion calculations were performed only for the upper core region.

In the XY plane, the superheater was divided into four regions, three fueled regions and the control rod channels. A two-dimensional void distribution was used in the boiler. The average of these voids was equal to the average voids at the axial height at which the superheater peak power occurs. Table I.3 lists the superheater average burnup and the XY peak-to-average power ratio from the upper core section as a function of core full-power days.

The XY and RZ results were synthesized to provide three-dimensional power distributions. These results are listed in Table I.4 in terms of superheater average burnup, peak burnup, and peak-to-average power ratio as a function of core full-power-days. The superheater peak-to-average power ratio decreases by approximately 10 per cent over the superheater life (10,000 MWD/t). Axial power distributions for the hot channel at the beginning of life and at 400 days are shown in Figure I.10. The small bumps at approximately 45 and 135 cm from the core top are caused by the boiler axial gaps. The dip and sudden rise from 100 to 80 cm are caused by the axial spacer plate in the superheater, and the change in baffle thickness and boiler lattice at the core axial mid-plane.

TABLE 1.3 SUPERHEATER XY DEPLETION STUDY

FULL POWER DAYS	AVERAGE BURNUP MWD/t	PEAK-TO-AVERAGE POWER RATIO
Upper Core Section		
0	-	1.530
200	6,290	1.405
400	13,870	1.452
Lower Core Section		
0	-	1.170

TABLE 1.4 SUPERHEATER BURNUP AND POWER DISTRIBUTION (SYNTHESIZED XYZ)

FULL POWER DAYS	AVERAGE BURNUP MWD/t	PEAK BURNUP MWD/t	PEAK-TO-AVERAGE POWER RATIO
0	-	-	2.01
200	6,000	11,700	1.94
400	12,200	22,300	1.83

TABLE 1.5 SUPERHEATER CHARACTERISTICS VERSUS CONTROL-ROD (SYNTHESIZED XYZ)

CONTROL ROD BANK DISTANCE FROM CORE TOP	k_{eff}	Δk_{eff}	STEAM TEMP. (°F)	ΔT °F	SUPERHEATER POWER FRACTION	PEAK-TO AVERAGE POWER RATIO
All Out	1.001	-	780	-	0.1924	2.00
18 in.	1.000	0.001	765	15	0.1863	2.25
36 in.	0.9955	0.0055	720	60	0.1648	2.35
All In	0.9822	0.0188	640	140	0.1209	2.47

1.6.1.2 Superheater Control-Rod Insertion. Synthesized XYZ power distributions for the beginning-of-life full-power equilibrium-xenon-and-samarium core were performed assuming superheater control rods at various insertions. The four rods were operated in a bank, withdrawn fully, and inserted 18 in., 36 in., and fully.

In XY geometry, the superheater rods were represented explicitly by effective diffusion constants in the fast group and a current-to-flux ratio in the thermal group. In RZ geometry, homogeneous two-group poisons were used. In the radial direction of the RZ problems, the control rod poisons were also homogenized but not into the outer row of superheater fuel elements. The superheater hot channel is in this row adjacent to the boiler.

The all-rods-out condition is the zero full-power-days case listed in Table 1.4 and illustrated on Figure 1.10. Additional calculations were performed for the superheater rods inserted to 18 in., 36 in., and full-in.

Table 1.5 lists the core multiplication constant, change in core multiplication constant (rod bank worth in Δk), bulk steam temperature, superheater power fraction, and peak-to-average power ratio as a function of control rod height. The superheater bulk steam temperatures and power fractions in Table 1.5 have been adjusted to core k_{eff} values of 1.0.

The axial power distribution for the superheater hot channel with the rods banked at 36 in. is illustrated in Figure 1.11. The all-rods-out case is the zero-days plot in Figure 1.10.

1.6.1.3 Development of Low-Enrichment Superheater Analytical Model. During the past two quarters, extensive measurements of the neutron flux distribution within the low-enrichment element have been made in the Allis-Chalmers Critical Experiment Facility (results are reported in ACNP-62005, Section 1.6.2). For

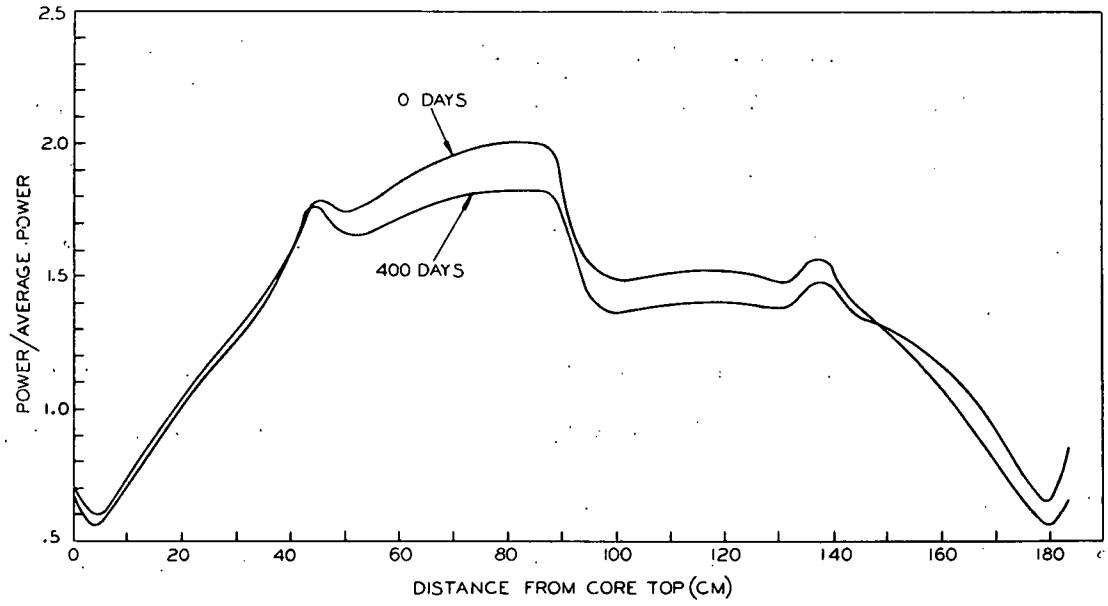

Figure 1.10 Low-enrichment superheater hot-channel axial power distribution with superheater control rods out. (A-C Dwg 43-025-138)

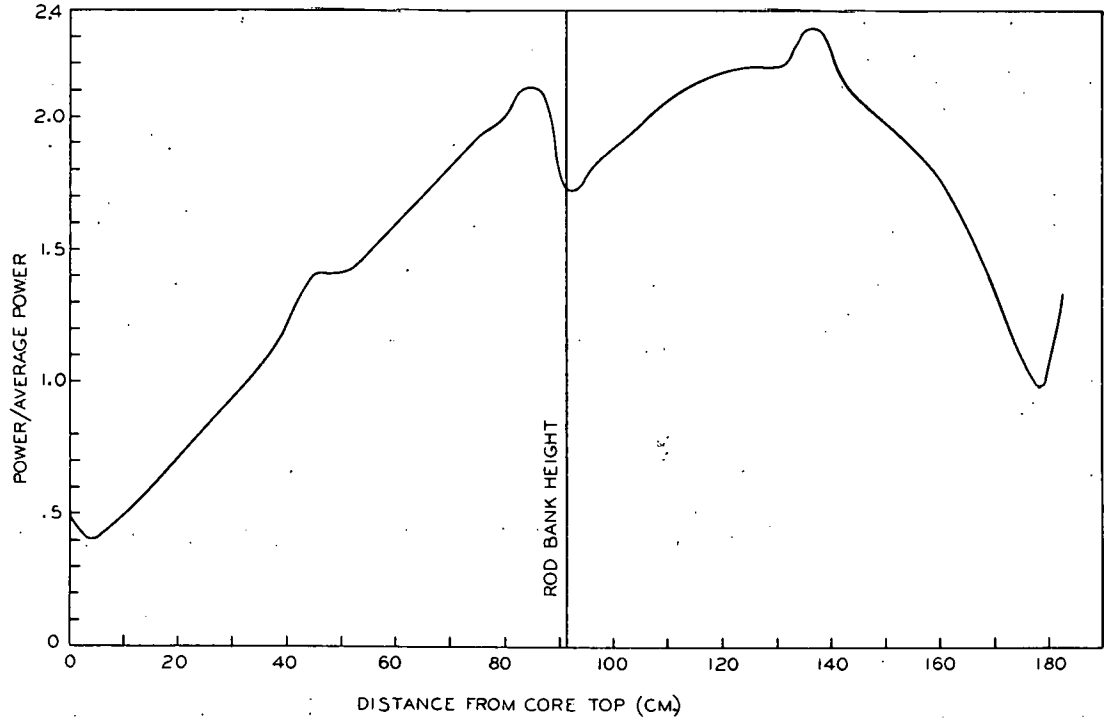

Figure 1.11 Low-enrichment superheater hot-channel axial power distribution with superheater control rods inserted 36 inches. (A-C Dwg 43-025-137)

these measurements, the following element parameters were varied (Figure I.12).

1) voided or flooded inside the outer stainless steel tube,

2) number of fuel rods per element (six or seven),

3) U-235 enrichment (3.5 or 7.0 w/o),

4) radial location of the outer six fuel rods (rod centers located on circles of radii of 0.2625, 0.2875, 0.325, and 0.375 in.) and

5) number of steel walls between fuel and moderator (one or two).

Activations were measured with U-235 foils. Cadmium ratios were measured to provide a determination of the epithermal and thermal activations, respectively, above and below a cutoff of 0.5 ev. Activation levels were measured in the following regions of the superheater fuel cell (Figure I.12):

1) fuel and clad,

2) moderator water (water outside outer steel wall),

3) double steel-wall region, and

4) non-fueled region inside inner steel wall (this region is either voided or flooded).

For comparison with the measured data, the flux distributions in the superheater element were computed by a straight forward application of the standard design model, as follows:

1) initial thermal spectrum calculation using SOFOCATE with volume-weighted number densities,

2) cylindrical P-3 six-region calculation (center fuel rod, void, outer fuel rods, void, double seal wall region, moderator), and

3) final thermal spectrum calculation with P-3 flux-weighted number densities.

In the cylindrical P-3 calculations, the water outside the outer steel wall was represented by an annulus. The outer fuel rods also formed an annulus one fuel rod in thickness with inner and outer boundaries tangential to the fuel rod surface. Fuel, clad, and void or water were homogenized together within this region.

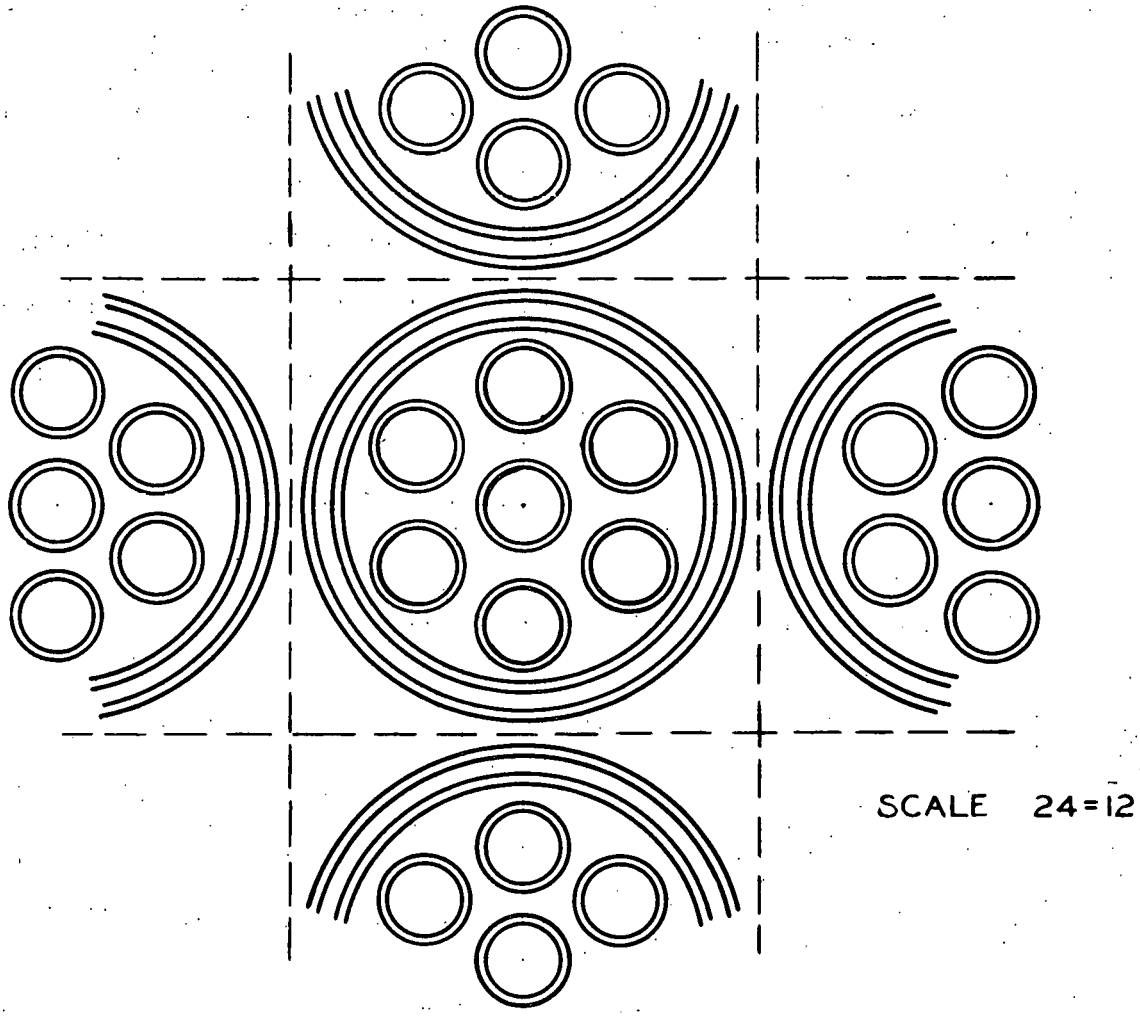

Figure 1.12 Critical facility low-enriched superheater element.
(A-C Dwg 43-024-917)

The measured thermal activations were used to provide weighting factors for the materials in the lattice. Thermal spectrum calculations were performed with SOFOCATE to a cutoff of 0.5 ev. As a comparison, between measured and calculated lattice parameters, the thermal multiplication factors (nf_2) with a 0.5-ev cutoff are listed in Table I.6.

The ABCD notation refers to the radial location of the outer fuel ring, radii of 0.2625, 0.2875, 0.325, and 0.375 in., respectively. The 1 and 2 notation refers to the number of steel walls between the fuel and moderator.

The flooded cases in Table I.6 use P-3 weighting in the outer fuel ring to weight the fuel, clad, and water together. The use of volume weighting within this annulua would increase the calculated nf_2 values by approximately 1.5 per cent.

The calculated values of nf_2 average about 2½ per cent higher than the measured values. The uncertainty in the measured values has not yet been calculated. Of interest in Table I.6 are:

1) the decrease in nf_2 with flooding,

2) the increase in nf_2 as the outer six fuel rods move outwardly decreasing their mutual shielding, and

3) the increase in nf_2 resulting from the removal of the inner steel wall.

Currently, several areas are being investigated. The spatial dependence of the thermal spectrum, especially for the voided cases, is being computed using the SLO-P-1[1]. SLO-P-1 will provide the U-235 fission activation to a 0.5-ev cutoff. Thus, ambiguity will not exist due to comparisons between increased U-235 activities and calculated fluxes. Unfortunately, since only a diffusion theory approximation is available in cylindrical geometry, the full extent of the thermal-spectrum effect on nf_2 will not be calculated.

(1) "SLO-P-1 -- A Thermal Multigroup Program for the IBM-704", WAPD-TM-188.

The second area being investigated is the effect of cylindricization, both of the moderator outside the steel wall and of the outer fuel rods plus associated flooding water. These effects are to be examined using transport theory for both the voided and flooded lattices.

TABLE 1.6 LOW-ENRICHMENT SUPERHEATER MEASURED AND CALCULATED THERMAL MULTIPLICATION FACTOR (nf_2)

LATTICE	MEASURED	CALCULATED	100X CALCULATED-MEASURED / MEASURED
7 Rod 3.5 w/o Voided	1.36		
A-1	1.362	1.402	2.9
B-1	1.371	1.407	2.6
C-1	1.374	1.414	2.9
D-1	1.381	1.422	2.9
B-2	1.222	1.267	3.6
C-2	1.236	1.275	3.1
7 Rod 3.5 w/o Flooded			
A-1	1.222	1.250	
B-1	1.238	1.262	1.9
C-1	1.262	1.279	1.4
D-1	1.287	1.298	.8
B-2	1.122	1.150	2.5
C-2	1.153	1.169	1.4
7 Rod 7.0 w/o Voided			
D-1	1.630	1.681	3.1
B-2	1.492	1.538	3.1
C-2	1.507	1.550	2.8
7 Rod 7.0 w/o Flooded			
D-1	1.557	1.565	0.5
B-2	1.398	1.406	0.6
C-2	1.430	1.449	1.3
6 Rod 3.5 w/o Voided			
D-1	1.349	1.389	2.9
B-2	1.182	1.224	3.6
C-2	1.192	1.234	3.6
6 Rod 3.5 w/o Flooded			
D-1	1.254	1.245	1.4
B-2	1.077	1.101	2.2
C-2	1.108	1.121	1.1

I.6.2 CRITICAL EXPERIMENTS

I.6.2.1 Flux Measurements in Low-Enriched Superheater Cells. The measurements of the regionwise thermal flux integrals for seven- and six-rod clusters of 3.5- and 7.0-per-cent enriched fuel have been completed. These cell measurements were performed to provide detailed data for use in the nuclear analysis of the low enriched superheater. The description of the experiment was detailed in ACNP-6123, and only a brief review of this description will be given here, along with a complete tabulation of results.

The average thermal-neutron activation flux in the following cell regions was made: 1) the central fuel rod (for seven-rod clusters) or the central space (for six-rod clusters); 2) the six outer fuel rods; 3) the moderator region exterior to the outer housing tube; and 4) seven concentric rings comprising the volume interior to the outer housing tube not occupied by fuel tubes. The dimensions of these cell regions are given in Table I.7 for the fuel rod spacings within the element under consideration. Each fuel rod is of 0.237-in o.d. with 0.214-in dia. fuel pellet and 0.010-in cladding. The fluxes given for the various rings in the fuel element represent the ring area minus whatever area is occupied by fuel rods in that ring. As the fuel rod spacing changes from B to C to D lattice, the areas left in the rings vary, but their position with respect to the cell center remains the same.

The measurements were performed by irradiating U-Al foil positioned in

TABLE I.7 FUEL-ROD AND RING POSITIONS

Regions	Outer Radius (inches)
Center Fuel Rod	0.119
Outer Fuel Rods	
Lattice B	(0.287)*
Lattice C	(0.325)*
Lattice D	(0.375)*
Ring 1	0.185
Ring 2	0.236
Ring 3	0.311
Ring 4	0.361
Ring 5	0.410
Ring 6	0.460
Ring 7	0.552
Moderator	[0.705]**

* (Radius of centers)
** [Effective radius]

the test element such that the entire cell area less the housing tube, which had to be kept intact, was represented by the foil. Of course, the plane of the foil was perpendicular to the axis of the fuel element.

Following irradiation, the positions corresponding to the fuel rods were punched out of the foil. The remaining foil was then punched into the seven ring-foils and the moderator foil. The gross beta fission-product activity of the foil sections was counted and recorded. Following a decay of at least one week, the foil sections were re-irradiated such that they all received the same integral flux exposure, and recounted in the same geometry and manner as before. This provided a calibration for each foil section which allows correction for size differences, foil inhomogenieties, and, for the most part, counting geometry.

After applying the results of cadmium-ratio measurements, the sub-cadmium or thermal activation flux for each cell region was obtained. These flux values are listed in Table I.8 for voided and flooded lattices of seven-rod fuel clusters. Variations in the seven rod clusters are the fuel enrichments of 3.5 and 7.0 per cent and the fuel rod spacing of B, C, or D. The errors assigned to these results are the most probable errors as determined from the analysis of the repetitive counts obtained on each foil. Repetitive measurements of several of the cases considered has established reproducibility to be within these quoted errors. Some of the results quoted here were given in ACNP-6123. They are repeated here for completeness and, because of slightly better cadmium-ratio measurements, the values have been altered slightly.

Listed in Table I.9 are similar results for six-rod lattices utilizing a fuel enrichment of 3.5 per cent. For purposes of checking the calculations, the fluxes for flooded case of the six-rod cluster were measured with the

TABLE I.8 MEASURED THERMAL FLUX IN SEVEN-ROD CLUSTERS

Location	B Lattice	C Lattice	D Lattice
1. Voided Lattice, 3.5 Per Cent Enrichment			
Center Fuel Rod	1.0000 ± .0063	1.0000 ± .0051	1.0000 ± .0051
Outer Fuel Rods	1.0803 ± .0061	1.0642 ± .0084	1.0597 ± .0062
Ring 1	1.0394 ± .0035	1.0551 ± .0040	1.0656 ± .0037
Ring 2	1.0682 ± .0069	1.0492 ± .0044	1.0770 ± .0061
Ring 3	1.1107 ± .0081	1.0720 ± .0044	1.0845 ± .0045
Ring 4	1.1796 ± .0045	1.1204 ± .0068	1.1107 ± .0070
Ring 5	1.2281 ± .0035	1.1614 ± .0037	1.1348 ± .0069
Ring 6	1.2760 ± .0062	1.1980 ± .0056	1.1823 ± .0043
Ring 7	1.3229 ± .0076	1.2549 ± .0063	1.2238 ± .0045
Moderator	1.6418 ± .0062	1.5644 ± .0072	1.5098 ± .0071
2. Flooded Lattice, 3.5 Per Cent Enrichment			
Center Fuel Rod	1.0000 ± .0045	1.0000 ± .0070	1.0000 ± .0052
Outer Fuel Rods	1.1197 ± .0053	1.1185 ± .0068	1.0767 ± .0063
Ring 1	1.0830 ± .0035	1.1119 ± .0063	1.1086 ± .0056
Ring 2	1.1287 ± .0057	1.1207 ± .0062	1.1412 ± .0066
Ring 3	1.1730 ± .0054	1.1587 ± .0069	1.1449 ± .0047
Ring 4	1.2702 ± .0062	1.2111 ± .0072	1.1636 ± .0079
Ring 5	1.3570 ± .0054	1.2767 ± .0062	1.1919 ± .0065
Ring 6	1.4550 ± .0081	1.3145 ± .0044	1.2427 ± .0067
Ring 7	1.5301 ± .0027	1.4032 ± .0096	1.2842 ± .0049
Moderator	1.7420 ± .0067	1.6274 ± .0062	1.4629 ± .0068
3. Voided Lattice, 7.0 Per Cent Enrichment			
Center Fuel Rod	1.0000 ± .0048	1.0000 ± .0050	1.0000 ± .0045
Outer Fuel Rods	1.1521 ± .0061	1.1009 ± .0050	1.0814 ± .0070
Ring 1	1.0642 ± .0036	1.1010 ± .0043	1.1036 ± .0044
Ring 2	1.0879 ± .0096	1.0832 ± .0054	1.1176 ± .0044
Ring 3	1.2053 ± .0060	1.1276 ± .0049	1.1097 ± .0044
Ring 4	1.3245 ± .0071	1.2170 ± .0056	1.1613 ± .0061
Ring 5	1.4221 ± .0057	1.2845 ± .0063	1.2040 ± .0057
Ring 6	1.5238 ± .0058	1.3513 ± .0037	1.2612 ± .0027
Ring 7	1.5858 ± .0058	1.4469 ± .0063	1.3401 ± .0047
Moderator	2.1235 ± .0069	1.9505 ± .0080	1.8116 ± .0074
4. Flooded Lattice, 7.0 Per Cent Enrichment			
Center Fuel Rod	1.0000 ± .0042	1.0000 ± .0048	1.0000 ± .0038
Outer Fuel Rods	1.1893 ± .0052	1.1490 ± .0048	1.1230 ± .0054
Ring 1	1.1119 ± .0038	1.1316 ± .0042	1.1900 ± .0057
Ring 2	1.1509 ± .0069	1.1413 ± .0046	1.2364 ± .0052
Ring 3	1.2851 ± .0075	1.2020 ± .0052	1.2367 ± .0031
Ring 4	1.4433 ± .0067	1.3163 ± .0065	1.2642 ± .0044
Ring 5	1.5813 ± .0057	1.4259 ± .0055	1.3294 ± .0044
Ring 6	1.7255 ± .0044	1.5176 ± .0073	1.4126 ± .0048
Ring 7	1.9027 ± .0062	1.6796 ± .0060	1.4897 ± .0057
Moderator	2.2577 ± .0073	2.0236 ± .0069	1.7976 ± .0075

TABLE I.9 MEASURED THERMAL FLUX IN SIX-ROD CLUSTERS

Location	B Lattice	C Lattice	D Lattice
1. Voided Lattice, 3.5 Per Cent Enrichment			
Fuel Rods	0.9709 ± .0057	0.9518 ± .0048	0.9439 ± .0064
Central Region	1.0000 ± .0058	1.0000 ± .0036	1.0000 ± .0047
Ring 1	0.9649 ± .0049	0.9847 ± .0039	0.9767 ± .0055
Ring 2	0.9637 ± .0063	0.9607 ± .0068	0.9628 ± .0062
Ring 3	1.0022 ± .0091	0.9774 ± .0086	0.9589 ± .0052
Ring 4	1.0423 ± .0034	1.0115 ± .0111	0.9769 ± .0085
Ring 5	1.0973 ± .0057	1.0335 ± .0066	0.9892 ± .0082
Ring 6	1.1164 ± .0078	1.0575 ± .0040	1.0211 ± .0049
Ring 7	1.1559 ± .0058	1.1003 ± .0048	1.0438 ± .0050
Moderator	1.4365 ± .0074	1.3780 ± .0065	1.3127 ± .0076
2. Flooded Lattice, Central Rod Position Flooded, 3.5 Per Cent Enrichment			
Fuel Rods	0.8418 ± .0066	0.8500 ± .0060	0.7956 ± .0052
Central Region	1.0000 ± .0056	1.0000 ± .0053	1.0000 ± .0074
Ring 1	0.8688 ± .0035	0.9625 ± .0038	0.9589 ± .0045
Ring 2	0.8683 ± .0079	0.9119 ± .0048	0.9314 ± .0043
Ring 3	0.8926 ± .0029	0.8963 ± .0076	0.8811 ± .0045
Ring 4	0.9571 ± .0069	0.9203 ± .0081	0.8759 ± .0082
Ring 5	1.0085 ± .0060	0.9488 ± .0076	0.8731 ± .0065
Ring 6	1.0606 ± .0047	0.9791 ± .0058	0.8995 ± .0069
Ring 7	1.1146 ± .0045	1.0264 ± .0063	0.9261 ± .0054
Moderator	1.2517 ± .0073	1.1763 ± .0063	1.0252 ± .0066
3. Flooded Lattice, Central Rod Position Voided, 3.5 Per Cent Enrichment			
Fuel Rods	0.9586 ± .0060	0.9076 ± .0061	0.8637 ± .0051
Central Region	1.0000 ± .0062	1.0000 ± .0065	1.0000 ± .0052
Ring 1	0.9722 ± .0043	0.9848 ± .0066	0.9972 ± .0063
Ring 2	0.9607 ± .0041	0.9567 ± .0056	0.9606 ± .0051
Ring 3	0.9863 ± .0071	0.9543 ± .0074	0.9372 ± .0040
Ring 4	1.0495 ± .0058	0.9843 ± .0080	0.9370 ± .0073
Ring 5	1.1153 ± .0047	1.0284 ± .0066	0.9512 ± .0054
Ring 6	1.1733 ± .0051	1.0050 ± .0049	0.9790 ± .0044
Ring 7	1.2411 ± .0047	1.1125 ± .0076	1.0070 ± .0052
Moderator	1.4124 ± .0055	1.2718 ± .0066	1.1297 ± .0062

central fuel-rod position, flooded and voided. The results of these measurements are shown graphically by Figures 1.13 through 1.19. Each figure shows the region average fluxes for the B, C, and D lattice of the test case represented. The points are plotted at the radial center of the corresponding region. Because it is difficult to assign a region to the outer fuel rods, their average flux value has been included as a separate point for each case. The flux in the rods is appreciably below that of the ring segments at the same radius, as expected, due to depression in the fuel. Arbitrarily, the average flux at the center of the cell is taken to be unity and all other fluxes are normalized to this value.

1.6.2.2. ρ^{28} Measurements in Low-Enriched Superheater Cells. The measurement of ρ^{28} (epi-cadmium to sub-cadmium U-238 activation ratio) was continued on flooded and voided lattices of 3.5- and 7.0-per-cent enriched superheater cells. Since these results are not yet complete, they will not be reported at this time. However, some alterations have been made in the experimental procedure, which is described in ACNP-62005, and these are as follows.

As described in ACNP-62005, the measurement of ρ^{28} consists of determining the cadmium-covered and aluminum-covered U-238 activation rate of a highly depleted uranium foil which is located in the fuel rod. The activity determination utilizes the U-239, 74-kev gamma ray, decay. Previous measurements have located a thin aluminum foil on each side of the depleted foil to catch fission recoil products which would affect the measured activity of the depleted foil after irradiation. Because the fuel rods used in these experiments are of relatively small diameter, 0.214-in dia., any streaming of resonance neutrons through the aluminum, which would

(Continued on page 49)

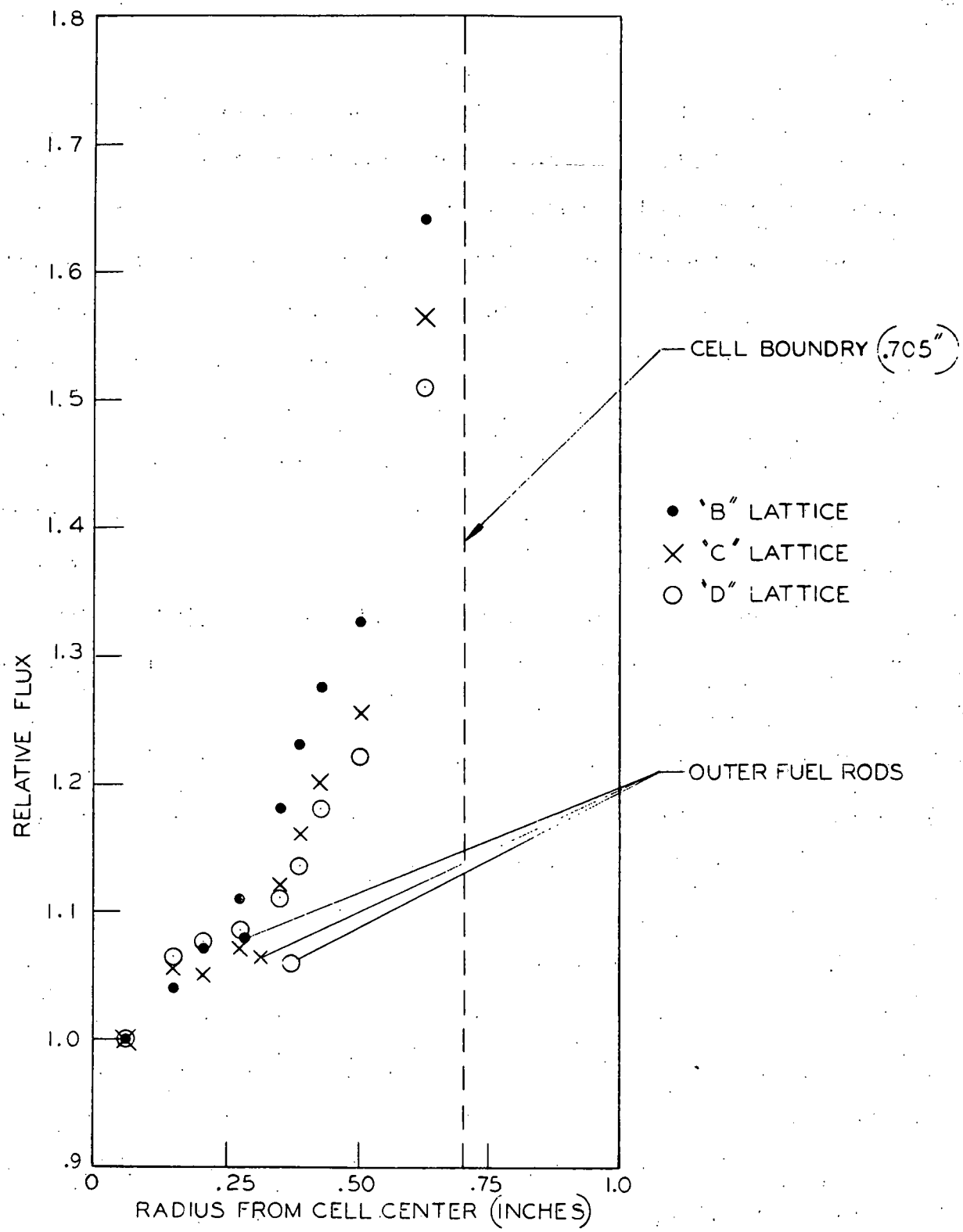

Figure 1.13 Measured thermal flux in seven-rod clusters (voided lattice, 3.5 percent enrichment). (A-C Dwg 43-025-127)

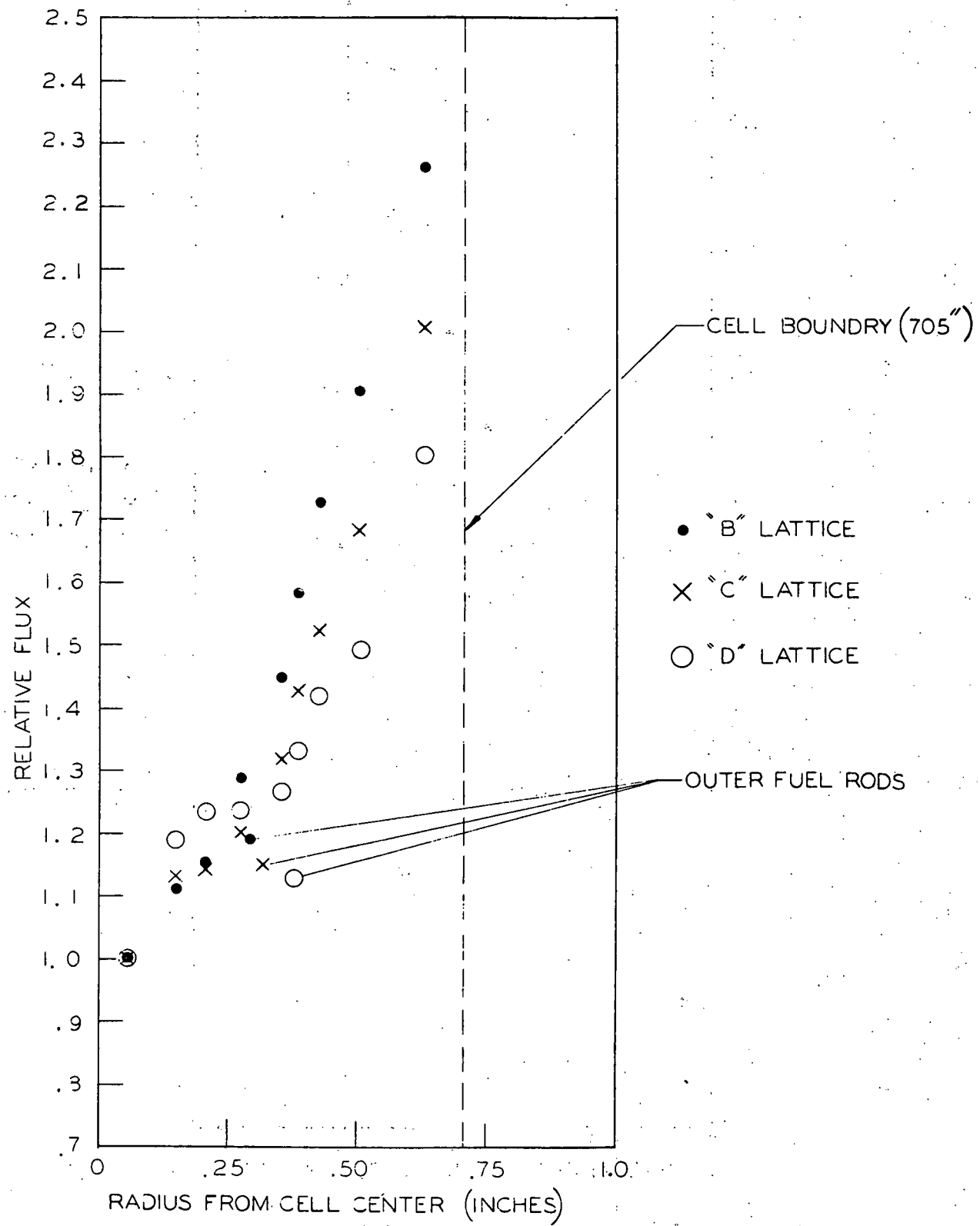

Figure 1.14 Measured thermal flux in seven-rod lattices (flooded lattice, 7.0 percent enrichment). (A-C Dwg 43-025-128)

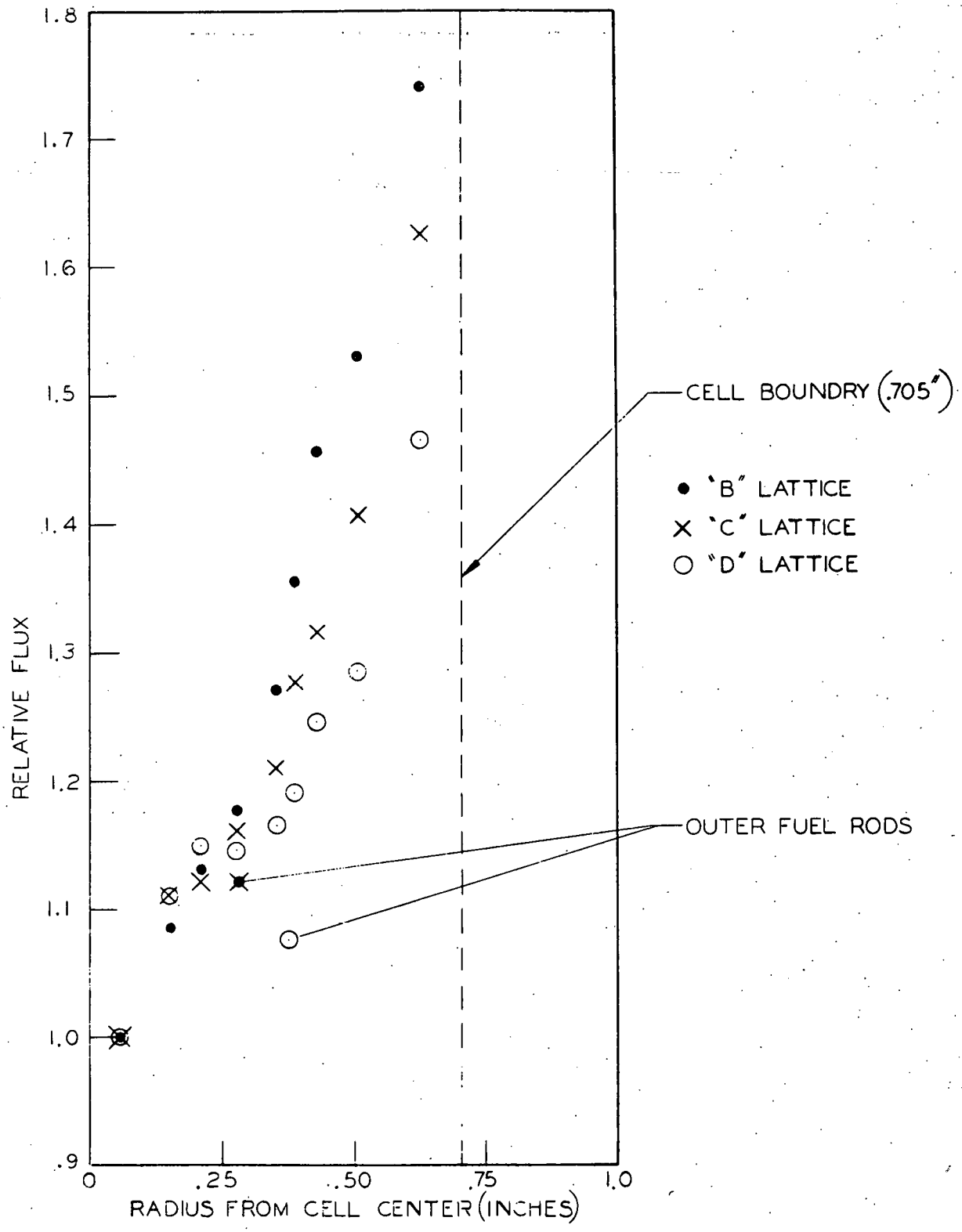

Figure 1.15 Measured thermal flux in seven-rod clusters (flooded lattice, 3.5 percent enrichment). (A-C Swg 43-025-129)

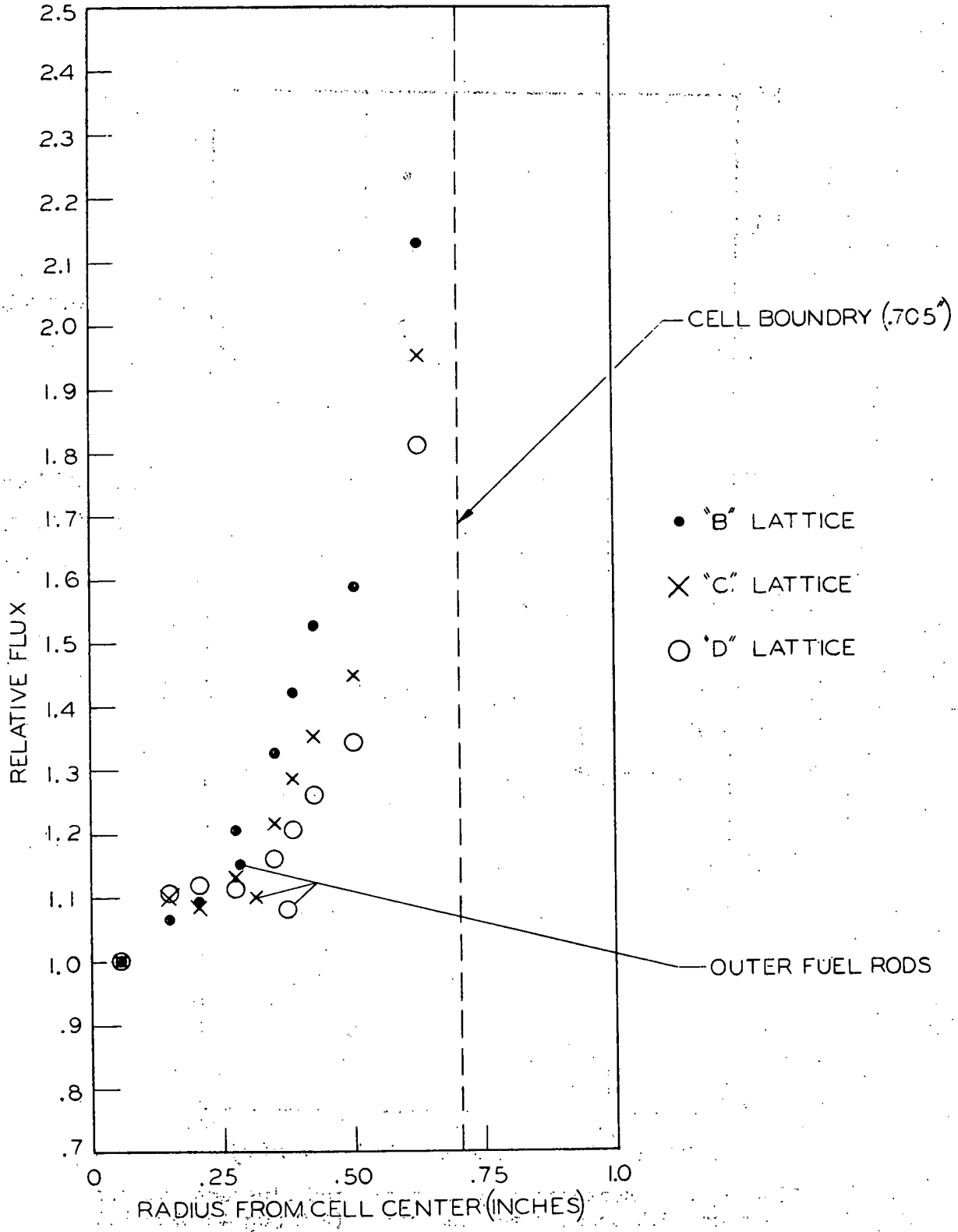

Figure 1.16 Measured thermal flux in seven-rod clusters (voided lattice, 7.0 percent enrichment). (A-C Dwg 43-025-130)

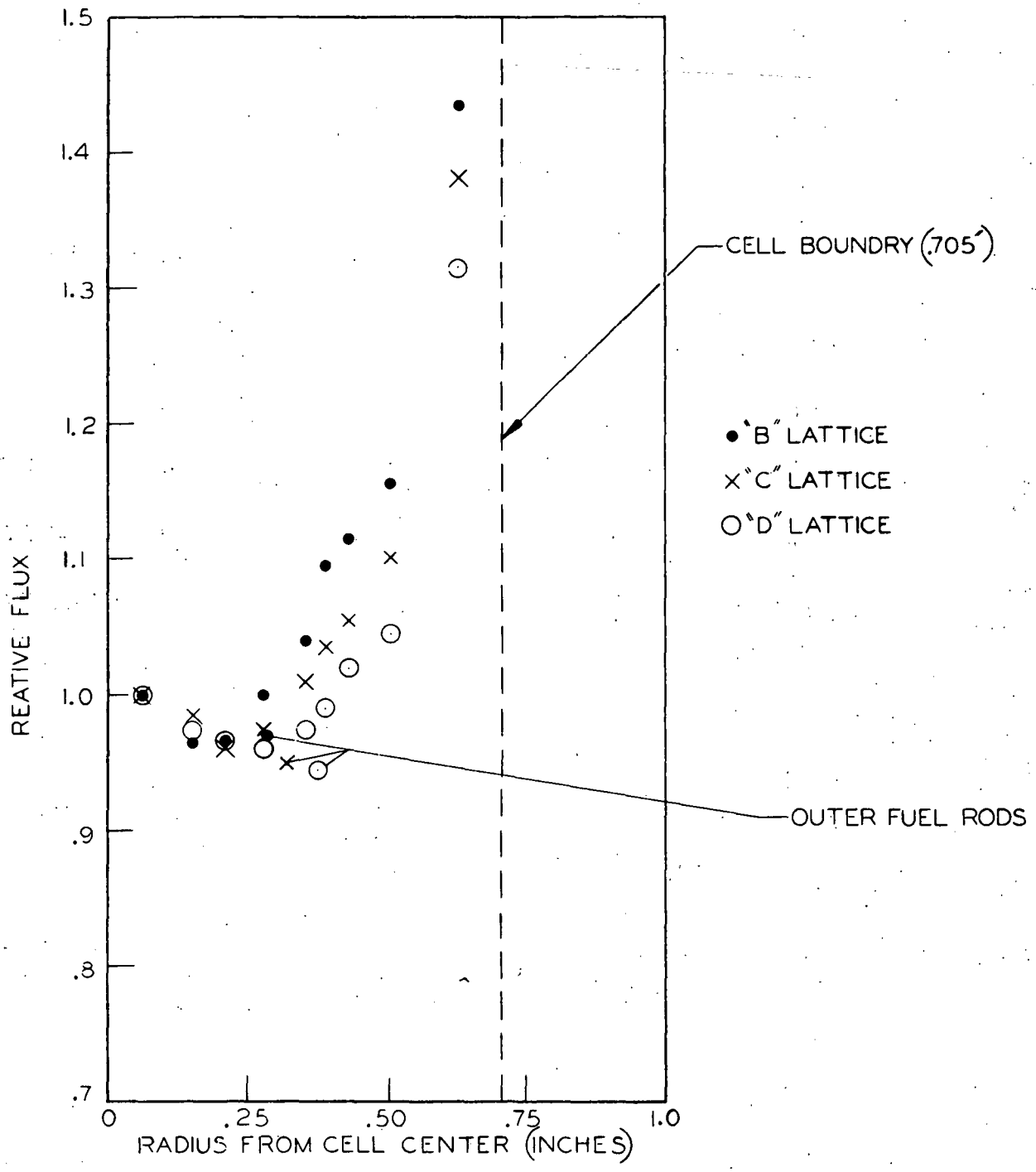

Figure 1.17 Measured fluxes in six-rod clusters (voided lattice, 3.5 percent enrichment). (A-C Dwg 43-025-131)

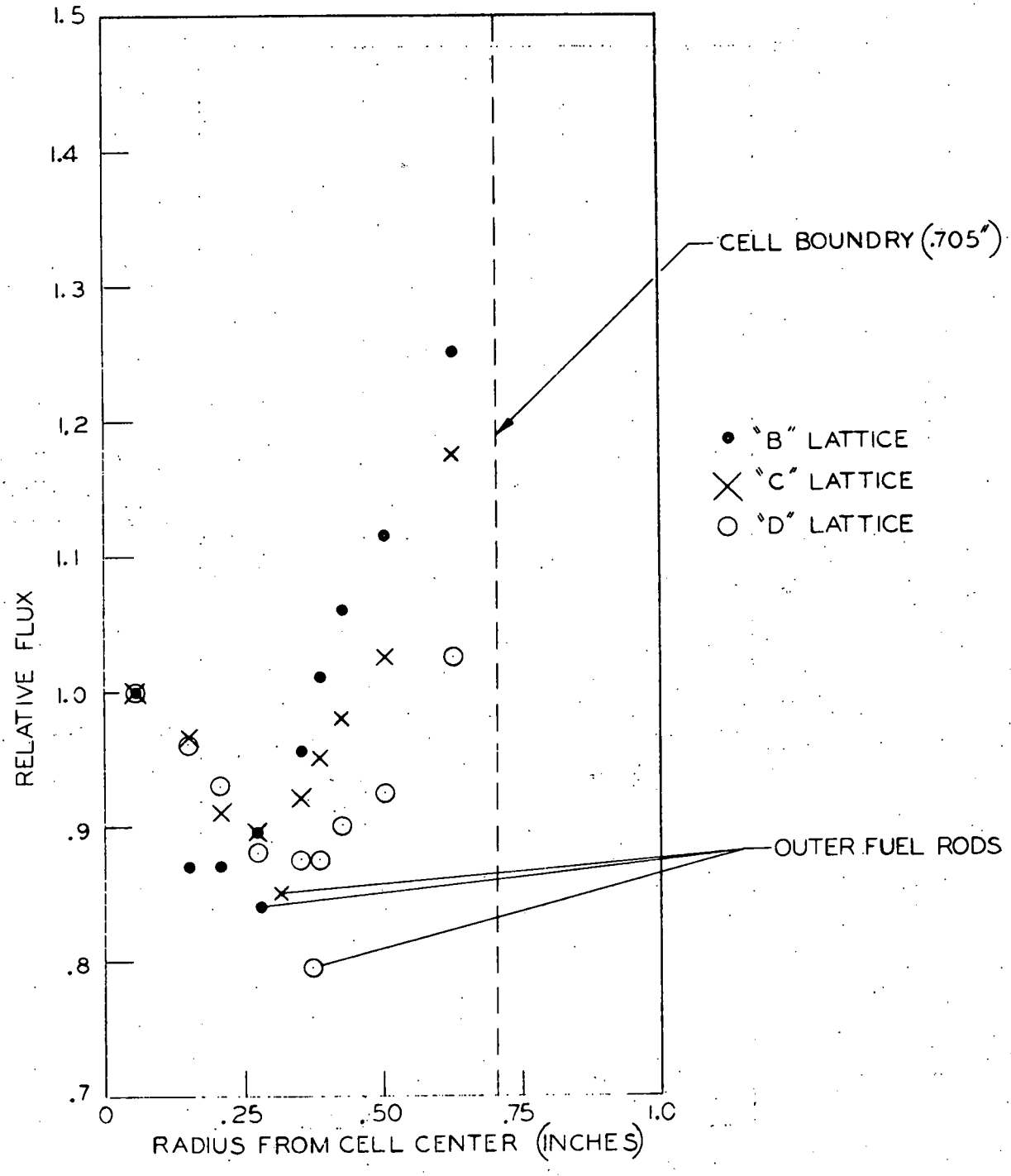

Figure 1.18 Measured thermal flux in six-rod clusters (flooded lattice, central-rod position flooded, 3.5 percent enrichment). (A-C Dwg 43-025-132)

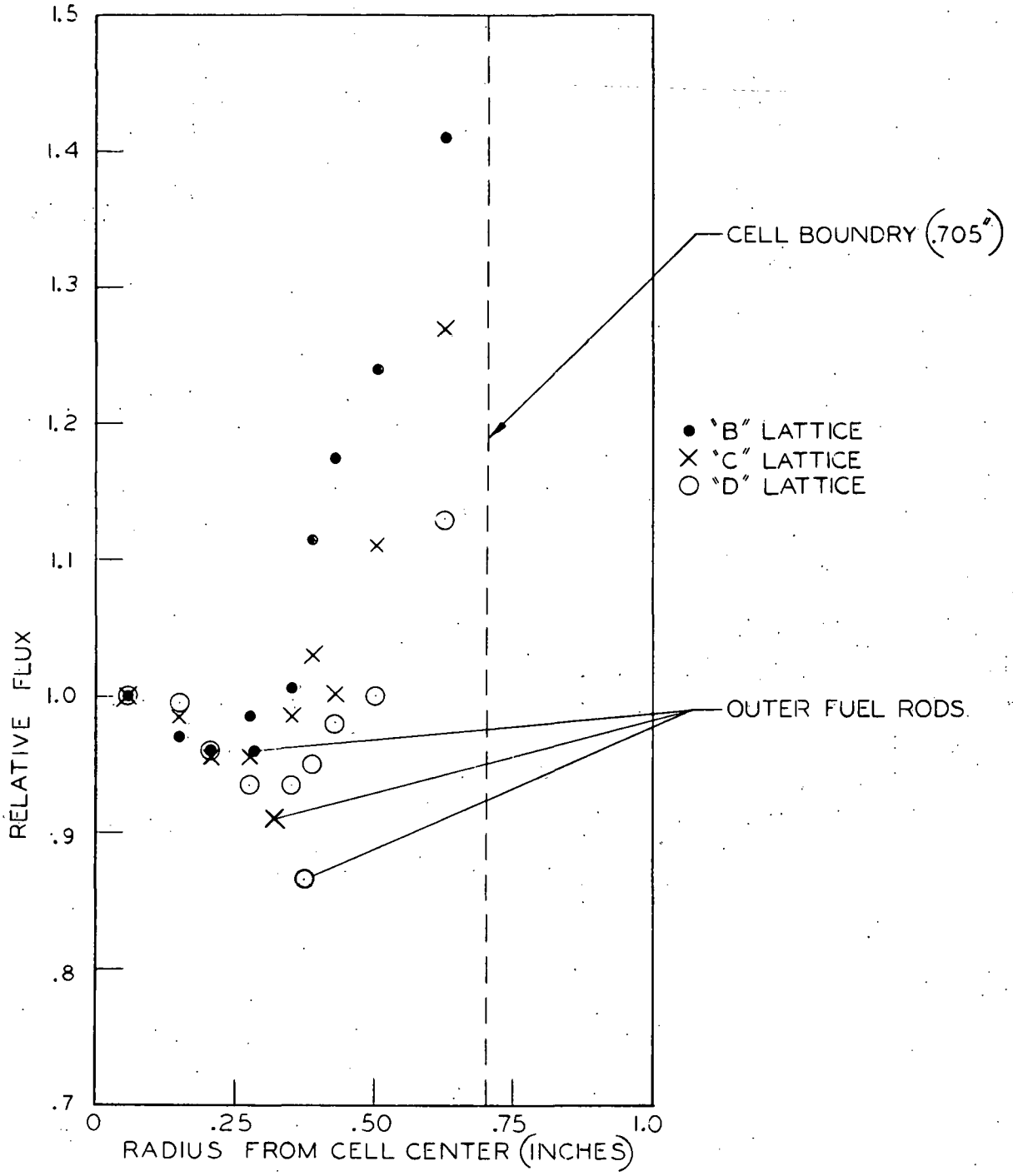

Figure 1.19 Measured thermal flux in six-rod clusters (flooded lattice, central-rod position voided, 3.5 percent enrichment). (A-C Dwg 43-025-133)

otherwise be absorbed on the surface of the uranium displaced by the aluminum, would cause a higher U-239 activity. Moreover, since the quantity, ρ^{28}, is formed by the ratio cadmium-covered activity to aluminum-covered- minus cadmium-covered activity, the excess activity would show up in the numerator but subtract out in the denominator, since neither the cadmium nor the aluminum will filter out these resonance energy neutrons.

This effect was measured by covering several depleted uranium foils with various thicknesses of aluminum, inserting them in a pellet stack, and exposing them to the same integrated flux. The resultant U-239 activity showed an increase corresponding to about 1 per cent per 0.001-in thickness of aluminum cover, i.e., if each side of the depleted foil was covered by a 0.001-in thick aluminum foil, the resultant activity would be 2 per cent high, extrapolating back to zero increased activity with no aluminum cover.

Because of this effect, and because of the possible difficulty in keeping close control of the separation of the fuel pellets and the depleted foil when an intermediate material is located in between, subsequent measurements have been performed without the aluminum catcher foil. To do this, measurements were made of the additional activity that would be contributed by fission products when the depleted foil was in intimate contact with the fuel pellets. This was done by irradiating aluminum foil in contact with the fuel pellets and counting the resultant aluminum caught fission product activity as a function of time (both for cadmium covered and bare pellet stacks) using the same spectrometer setup as is used for the U-239 counting. This activity is now subtracted as background from the measured activity of the irradiated, unprotected depleted foils.

1.6.3 HEAT TRANSFER AND FLUID FLOW

1.6.3.1 Air-Flow Tests. Tests were conducted on several low-enrichment superheater ferrule-spacer designs to determine the effect of axial interval between spacers on the spacer loss coefficient and to determine values of the spacer loss coefficients. The tests were conducted in an open flow loop with air at approximately 100 psia and room temperature.

The test section was built to the approximate dimensions of the fuel element and process tube designed for Pathfinder. The seven-rod fuel element cluster was fabricated from 0.249-in dia. ground stainless-steel rods 76-in long held at each end by special fittings. The centers of the six peripheral rods were located on a circle of 0.593-in dia. The process tube, which also served as the pressure housing, was 0.944-in i.d.

Two spacers, shown in Figure 1.20 were studied with this test section. The first consisted of smooth ferrules of 0.343-in o.d. fitting over each of six peripheral rods in positions on a spiral about the axis of the fuel element. The second spacer consisted of a ring over the peripheral rods which held the rods in contact with a 0.343-in o.d. ferrule on the center rod.

The results of these tests are presented as loss coefficients versus Reynolds numbers in Figure 1.22 and 1.23. The loss coefficient represent the average loss that may be attributed to a single spacer, i.e. K_R is the loss coefficient associated with one ring-and-center-rod-ferrule spacer, and K_F is the loss coefficient associated with an individual ferrule located on a peripheral rod. These coefficients act on the average velocity head of the gas in the unrestricted flow area.

Separate tests of the ring-and-center-rod-ferrule spacer showed an average loss coefficient of 2.24.

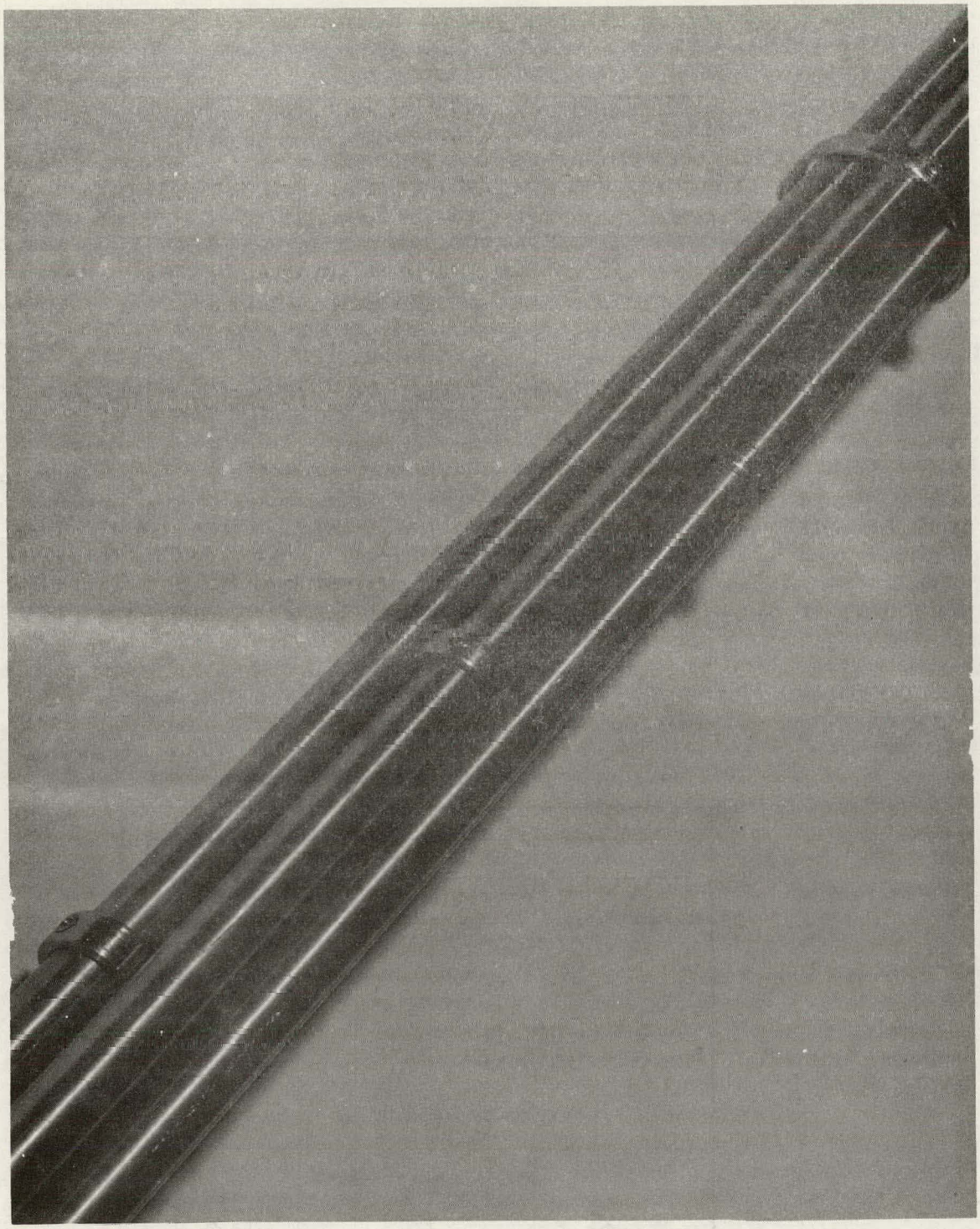

Figure I.20 Peripheral ferrule spacer and ring-and-ferrule spacer for the low-enrichment superheater fuel element.

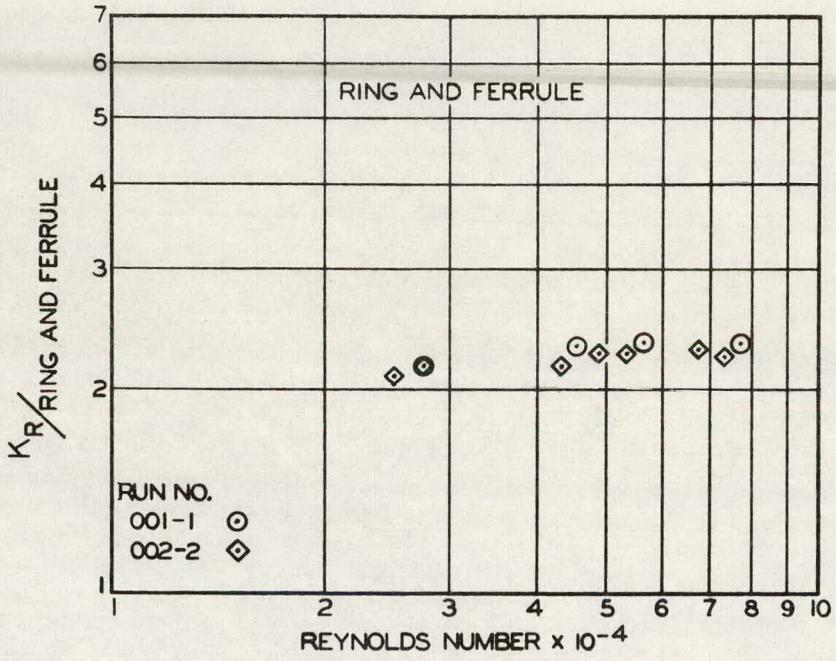

Figure 1.21 Loss coefficient for ring-and-ferrule spacer.

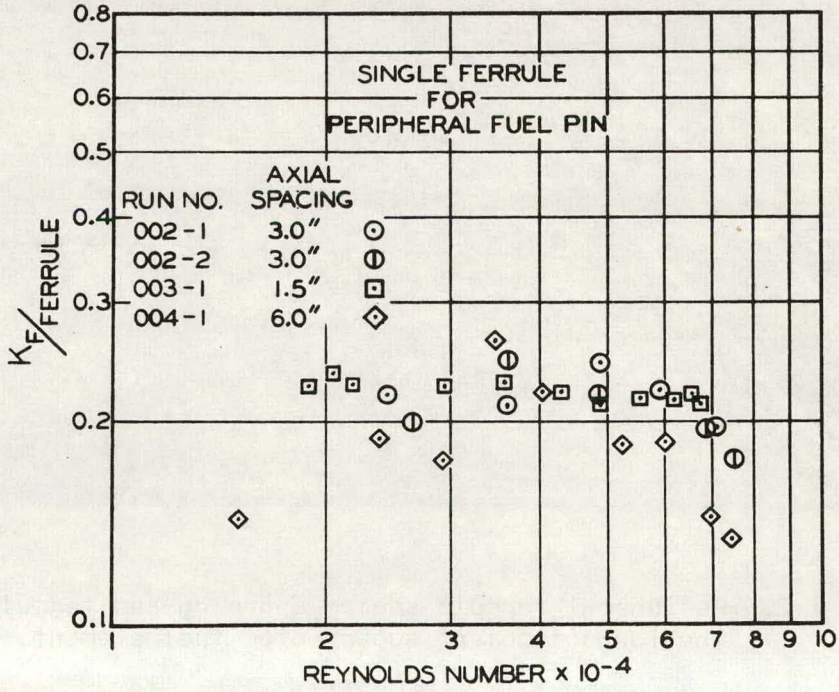

Figure 1.22 Loss coefficient for peripheral ferrule spacer.

Tests of elements were then conducted to determine loss coefficients of peripheral ferrules with the ferrules at axial intervals of 9 to 35 equivalent diameters (1.5, 3, and 6 in intervals). The tests indicated no interaction between ferrules at these intervals. The average value of the loss coefficient for the peripheral ferrule is 0.22. This loss coefficient is about 43 per cent greater than loss coefficients predicted from published values of contraction and expansion losses for concentric pipe.

Additional tests of a third spacer design were initiated. This spacer design consists of three ferrules on alternate peripheral rods at the same axial location. Initial tests showed a loss coefficient of about 1.1 for Reynolds numbers 30,000 to 70,000.

1.6.4 FUEL FABRICATION RESEARCH

Investigations are being conducted to develop economical methods of fabricating high-density uranium dioxide fuel rods with limited interconnected porosity for good heat transfer and retention of fission gases. Work during this quarter has continued on fuel elements produced by swage-compaction and collapse cladding over sintered pellets.

1.6.4.1 Swage-Compacted Fuel Rods. Work reported in the last quarterly report showed that 75 w/o arc-fused and 25 w/o ceramic grade powder would swage to a maximum density of 88 per cent of theoretical. Fuel rods with a minimum density of 90 per cent theoretical are the objective.

Primary effort during the quarter was to obtain a swaged fuel-rod density of 90 per cent theoretical by using 100 per cent arc-fused -20 mesh as-received powders. Preliminary work had indicated that this might be possible.

Swaged-Density Characteristics of -20-mesh Arc-Fused Powders. Sixteen fuel rods were fabricated of -20 mesh as-received arc-fused powder with all processing variables kept constant except the amount of reduction, which was varied from 21 to 60 per cent. The literature had indicated that a prefiring of the as-received arc-fused powder would decrease comminution during vibratory compaction and, therefore, produce more control in the preswaged rod density. Therefore, the -20 mesh arc-fused powder was fired in a hydrogen atmosphere for 2 hr at 1700 C. The firing reduced the particle size as shown in Table 1.10. The cladding used was 316L stainless steel of 0.325-in o.d. with 0.010-in wall thickness. The rods were vibrated on a pneumatic air vibrator to 70.4 to 71.6 per cent of theoretical density. The rods were swaged at a rotational speed of 35 rpm while being fed into the swager at 2.7 in/min.

Partial evaluation of the rods is shown in Table 1.11 and Figure 1.23. Standard evaluation techniques described in previous reports were used for this work. The vibrated density of rods produced with the prefired powder varied 1.25 per cent. This was a great reduction in the variation of vibrated rod density compared to previous work. The prefiring of the as-received arc- fused powder apparently produced a more stable powder for vibratory compaction.

The maximum swaged density of the rods was slightly less than 90 per cent of theoretical. The rod density is very uniform except for rods swaged to a reduction of 47 per cent. This variation in density is probably the result of a rapid density increase in this range. The data also shows overswaging at reductions of 55 per cent or greater. The amount of elongation for the various reductions produced a very reliable curve for predicting

TABLE I.10 PARTICLE SIZE DISTRIBUTION OF ARC-FUSED UO_2 POWDER USED FOR SWAGING STUDY

Particle Size*	As Received w/o	Fired** w/o
-20 + 70	68.8	53.6
-70 + 80	2.4	0.6
-80 + 100	5.6	7.0
-100 + 120	2.2	3.8
-120 + 140	2.9	5.7
-140 + 170	1.3	2.7
-170 + 200	2.2	3.8
-200 + 230	1.9	3.9
-230 + 270	1.0	1.9
-270 + 325	2.4	3.1
-325 + 400	0.7	1.2
-400	8.6	12.8

* U.S. Standard Sieve Size
** Fired at 1700C for 2 hrs.

TABLE I.11 PROPERTIES OF VIBRATORY COMPACTED AND SWAGED UO_2 FUEL RODS WITH 100 PER CENT ARC-FUSED POWDER

Rod No.	Vibrated Density (% TD)	Vibrating Time[1] (min.)	SWAGE Red. (%)	Swage Density (% TD)	Variation in Rod Density (%)	Elong. %
1	71.66	5	21.04	----(2)	------	7.53
2	70.73	5	21.04	-------	------	7.64
5	70.74	5½	30.47	88.75	0.56	19.34
6	70.41	6	30.57	88.85	0.53	18.71
7	71.50	5	33.00	88.93	1.41[3]	23.90
8	70.81	6	33.63	89.69	0.24	21.69
11	71.18	6	40.20	88.89	0.07	44.62
12	70.73	5½	41.07	88.72	0.25	40.54
13	70.69	5	47.18	88.36	1.10	59.40
14	71.77	5	47.29	88.83	2.19	60.60
15	70.61	5½	51.28	90.12	0.25	67.92
16	70.43	5½	51.33	89.67	0.56	70.45
17	71.03	6	55.55	88.48	0.50	90.09
18	70.76	6	54.35	88.51	0.05	86.67
19	70.87	5	59.52	87.14	0.84	115.25
20	70.89	6	59.55	87.20	0.39	110.24

1. 1-1/4 in. piston pneumatic vibrator operated at 80 psi
2. Powder was loose and density could not be determined
3. Error made in cutting density specimens, therefore, results not too accurate.

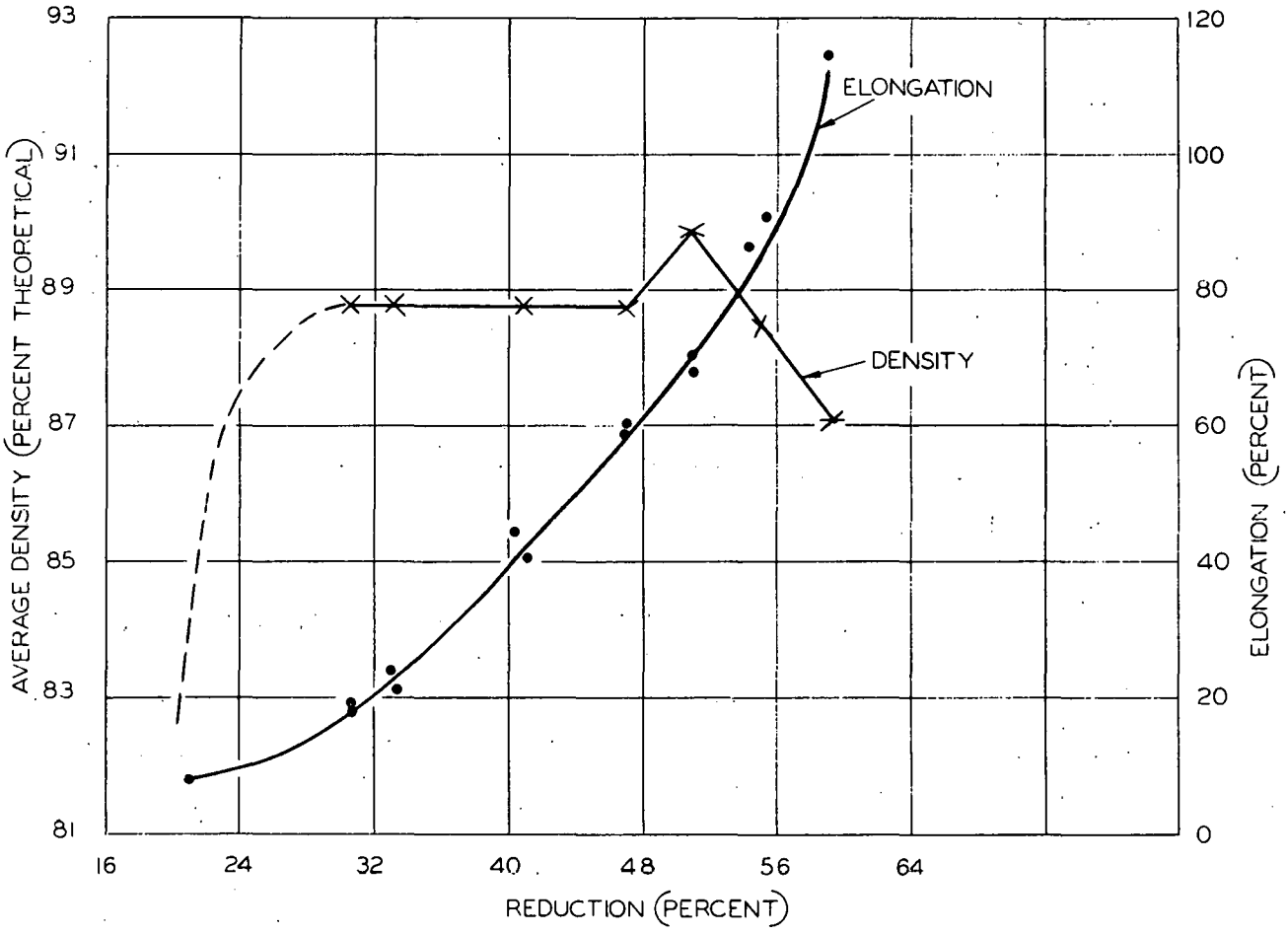

Figure 1.23 Average fuel density and rod elongation as a function of swaged reduction. (A-C Dwg 43-025-114)

rod lengths for a given reduction.

More study of reductions of this powder from 46 to 52 per cent is necessary to determine if the density of 90 per cent theoretical can be obtained. Such a study is advisable because of the cost savings that would result if fractionation of the powders is not necessary. Completion of the evaluation on these rods, however, is the only work presently planned for this project.

1.6.4.2. Clad-Bonding Studies. Investigations were continued during the quarter to determine optimum draw- and stretch-bonding parameters for producing high-density fuel elements using 0.010-in thick cladding. Studies of draw lubricants and draw speeds were performed to determine if pellet separation or damage could be reduced. The stretch-bonding process was modified to permit application of mandrel pressure on both ends of the pellet stack, and rods were sucessfully fabricated using this modified process. Clad-bonding studies using 0.013-in thick clad, which is being considered for use in Pathfinder, were initiated.

Draw-Bonding. Initial experiments to determine the effect of draw speeds and lubricants on pellet separation and damage were conducted. A series of rods were drawn using various lubricants at draw speeds from 8 to 72 in/min. X-ray and density evaluation did not indicate any significant change in pellet separation or damage.

Investigations of the draw characteristics of 0.013-in thick cladding were initiated. Two rods were drawn to 2.7 and 4.2 per cent reduction in area. The rod reduced 4.2 per cent exhibited severe pellet damage. At 2.7 per cent reduction in area, pellet damage was not significant. Density

measurements are being made.

Work during the next quarter will involve use of a mandrel that will apply an axial load to the pellet stack to determine if the pellet separation, damage, and rod density can be improved.

Stretch-Bonding. Investigations were initiated to study various gripping end caps which would permit application of mandrel pressure to both ends of the pellet stack during stretch bonding. Analysis led to the use of hollow butt-welded and shoulder-welded gripping end caps. Both designs were capable of reducing stress concentrations, hence premature clad failure, by providing a transition zone for the stretch forces.

Four 29-in long rods of 0.013-in thick cladding were stretched with hollow gripping fixtures and the double mandrel. The use of shoulder-welded end caps (Figure I.24) permitted sucessful stretching to the 1.5 per cent elongation required to attain pellet contact. Evaluation showed negligible pellet separation with intimate clad-pellet contact over the entire length.

An experiment was initiated to stretch 6-ft long fuel rods. One 6-ft long rod was prepared with 0.013-in thick walled tubing with shoulder welded gripping end caps. The rod was stretched 1-7/16 in, 2 per cent elongation, to clad failure. Reduction in area was not uniform over the 6-ft length. Pellet contact was achieved at the draw end of the rod but showed a 0.0005-in clearance at the fixed end (Figure I.25). A 0.068-in difference in elongation per 5-in increment was noted between the fixed end and draw end of the rod. Pellet separation was negligible.

Evaluation indicated that contact first occurs at the draw end and that frictional resistance between the mandrel-fixed pellet stack and clad

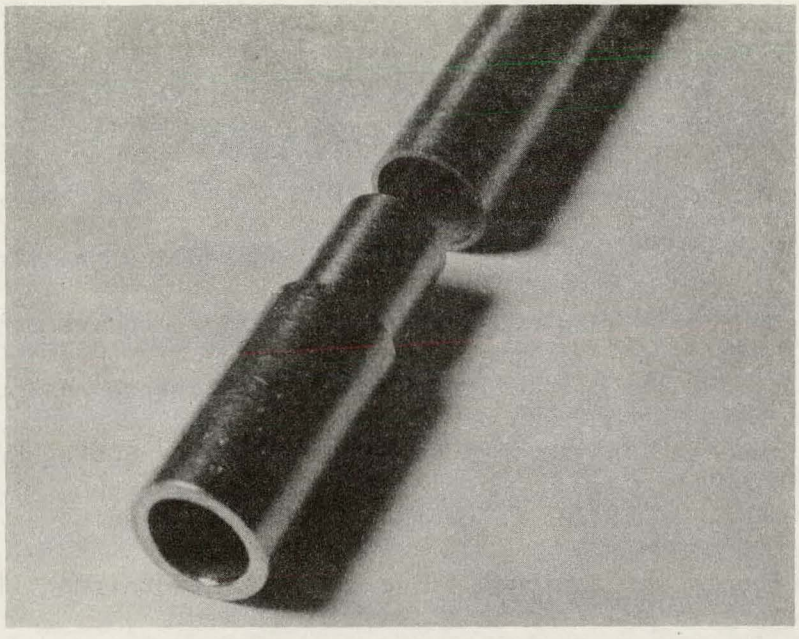

Figure 1.24 Typical shoulder-weld end cap for stretch bonding.

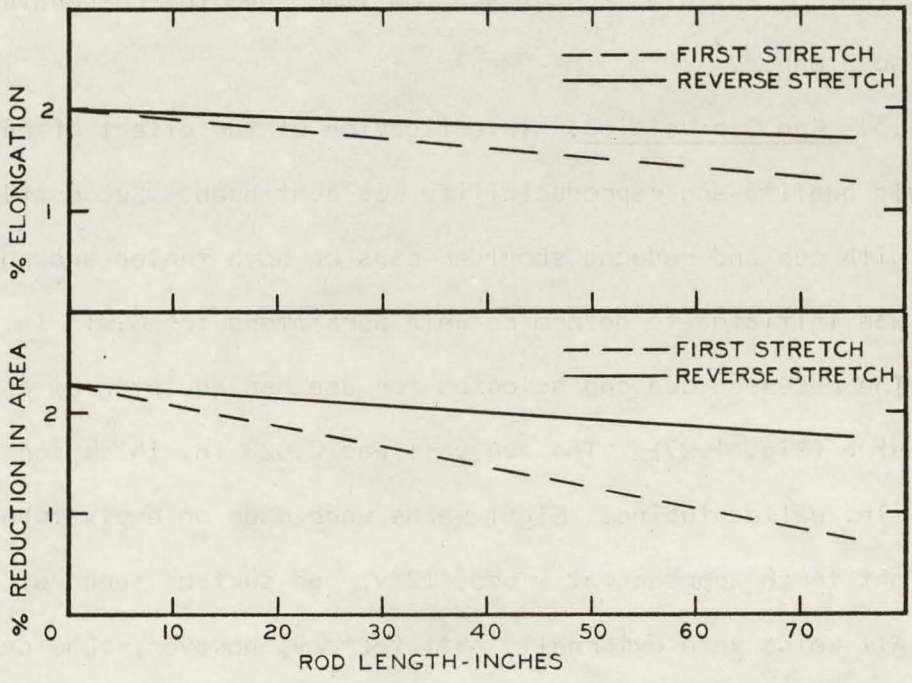

Figure 1.25 Elongation and reduction in area over the rod length during stretch bonding. (A-C Dwg 43-025-054)

increased as more contact was achieved toward the fixed end. Failure occurred at the draw end before complete contact was made, (Fig. I.26) due to clad reduction between the gripping end cap and the first pellet.

A second 6 ft long rod was prepared. The rod was stretched 1½ in. at one end, and the elongation and diametral change was noted. The rod was then reversed in the fixture and stretched. Subsequent dimensional analysis (Fig. I.25) indicated that intimate contact over the entire 6 ft rod length was achieved. Evaluation of clad integrity and grain size is being made.

Future work will involve studies of a mandrel with a collapsible end that will size the end of the tube for the fuel rod end cap, and that will be easily removable. Performance of a reproducibility run using the collapsible mandrel and the improved stretch-bonding methods is also planned.

I.6.4.3. End Cap Welding. Investigation of the effect of end-cap design on weld quality and reproducibility was continued. Successful runs were made with cup and reduced shoulder caps on both fueled and non-fueled tubes. Work was initiated to determine weld parameters for 0.013 in. walled tubes.

The recessed cup cap selected for use had an integral assembly attachment stub (Fig. I.27). The cup wall was 0.020 in. thick for use with 0.010 in. walled tubing. Eight welds were made on empty tubes using a straight torch approach at 9 amp, 12 v, and surface speed of 14 in/min.

All welds were externally satisfactory, however, tube ovality resulted in slight variations in puddle width. Destructive evaluation showed average penetration of 0.020 in. with minimum penetration equal to wall thickness. No evidence of porosity was observed, but significant quantities of finely

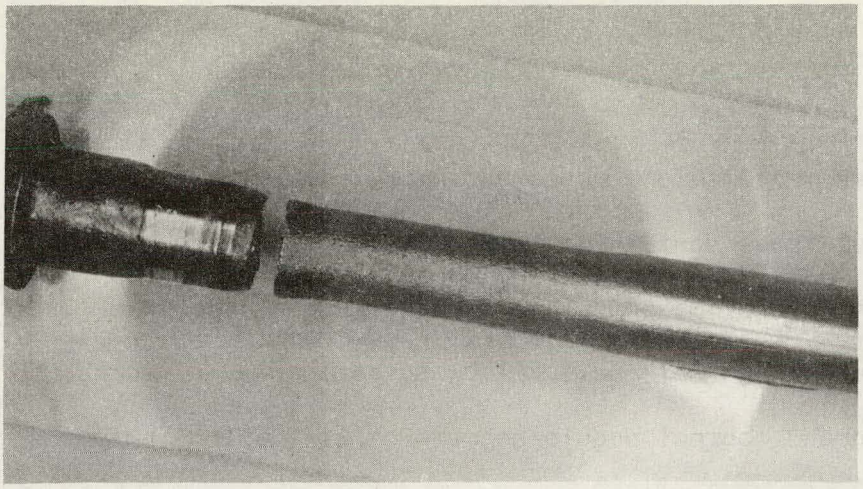

Figure I.26 Typical premature fracture observed at draw end of 6-ft long fuel rod during stretch bonding operation.

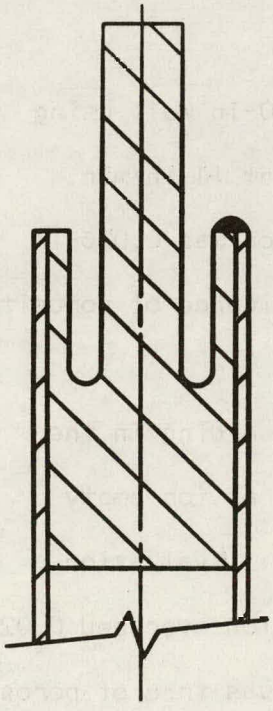

Figure I.27 Schematic of recessed cup-cap.

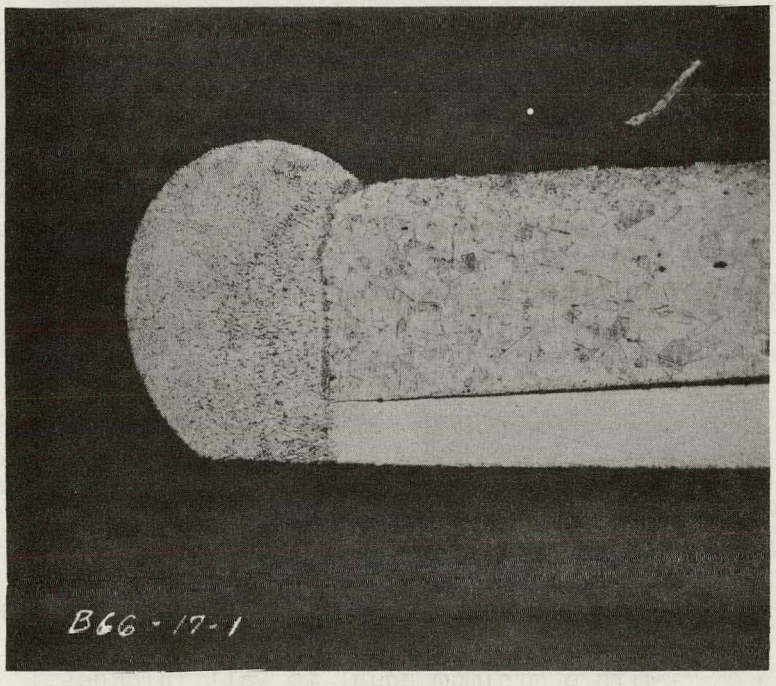

Figure I.28 Typical weld zone on recessed cup-cap.

dispersed ferrite were observed in the heat-affected zone (Figure I.28).

Four tubes containing swaged UO_2 were prepared for welding by leaching and reaming the rod ends. Welds were made at the same conditions used for empty tubes. An external chill was used, however, to reduce ferrite precipitation and control puddle geometry. Evaluation indicates that these welds would be satisfactory. Penetration averaged 0.018 in. with a minimum equal to the tube wall. Weld puddle geometry and microstructure were satisfactory (Figure I.29).

A similar experiment was performed using an end cap designed with a reduced shoulder cap, (Figure I.30). The initial design selected had a shoulder measuring 1/16 in. across the face. Preliminary studies showed that shoulder width and mass were too great resulting in a poor heat balance during the weld. Consequently, an end cap with a 1/32-in wide shoulder was used in subsequent welds.

Six weld samples were made on empty tubes with 0.010-in wall using an external chill. Welds were made using 19 amp, 12 v, at 14 in/min. All welds appeared satisfactory. Average weld penetration was 0.026-in with minimum penetration equal to wall thickness. No evidence of porosity or ferrite was observed.

Four tubes containing swaged UO_2 were prepared for welding in the manner used for cup caps. Parameters used were the same as for empty tubes except for amperage, which was increased to 22 amp. Evaluation indicated that the welds were also acceptable. Penetration averaged 0.024 in. with a minimum equal to wall thickness. Microstructure was free of porosity and showed no evidence of contamination. (Figure I.31).

These experiments indicate that a combination of weld parameters and

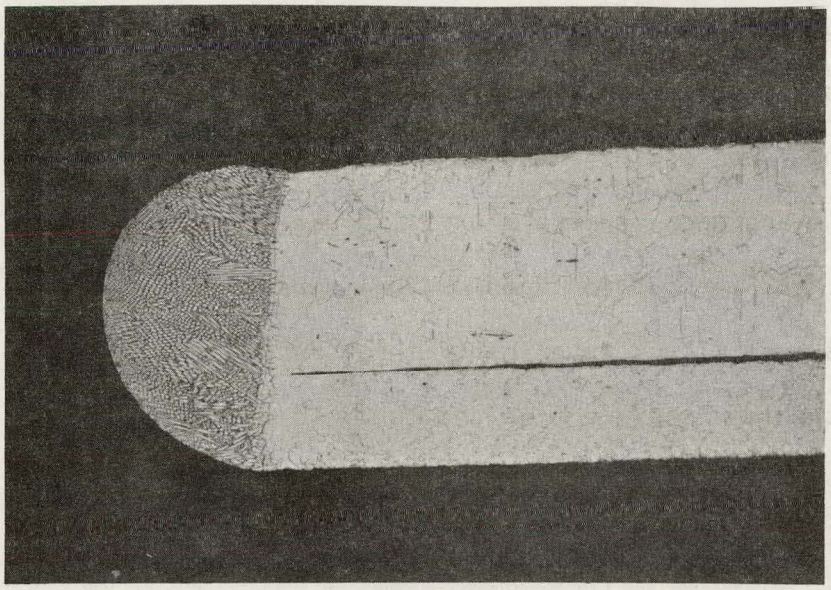

Figure 1.29 Typical weld zone on recessed cup-cap using external chill to reduce ferrite formation.

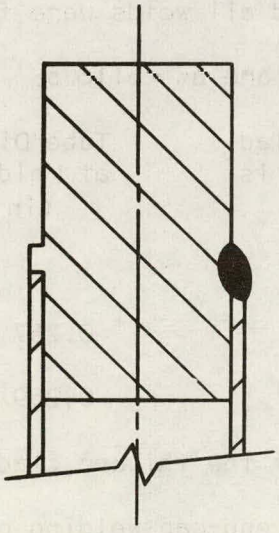

Figure 1.30 Schematic of reduced shoulder cap.

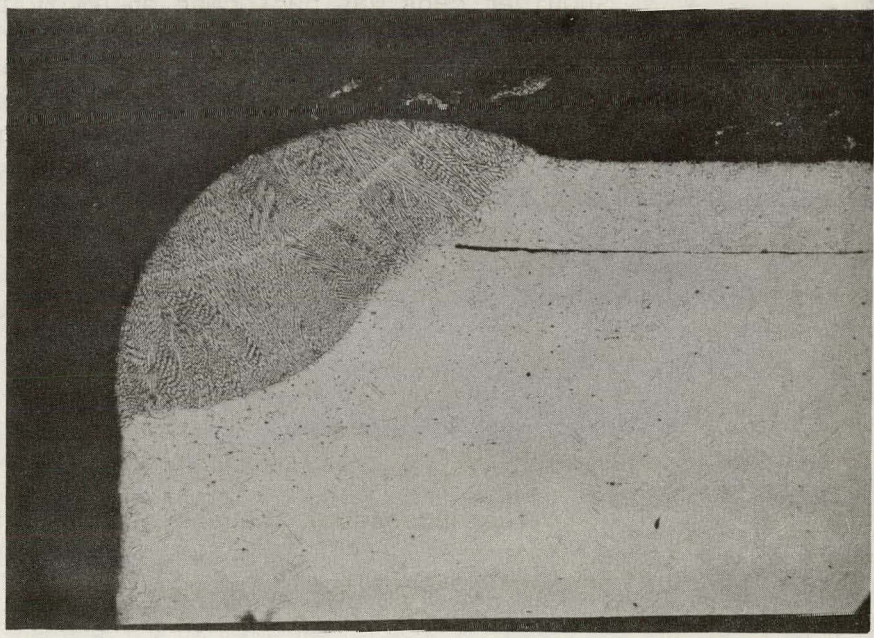

Figure 1.31 Typical weld of reduced shoulder cap to 0.010 in. tube wall

end-cap design can be selected to produce consistently sound welds for Pathfinder. The tentative reference process will use a reduced shoulder cap at the lower end of the assembly and a recessed cup cap at the upper end. This approach is consistent with designs for the upper and lower end fittings, and methods for spacing fuel pins in the assemblies.

In a preliminary experiment, three recessed cup caps and three reduced shoulder caps were welded to 0.013 in. walled tubing. Weld speed, voltage, and chills were identical to those used for 0.010 in. walled tubing. Amperages used were 9, 11, and 13 amp for recessed cup caps, and 21, 23, and 25 amp for reduced shoulder caps. External appearance of all welds was satisfactory. Optimum amperage was 12 amp for the recessed cup cap and 23 amp for the reduced shoulder caps.

A reproducibility run of six recessed cup caps and six reduced shoulder caps was performed on empty tubes. External appearance of all welds was satisfactory. Destructive tests showed all welds were free of porosity and contamination. Dimensional results are as follows:

Type	Penetration (in.)		Minimum Clad thickness is weld zone (in.)	Tube Diameter at Weld Bead (in.)
	Average	Range		
Cup	0.020	0.017-0.024	0.013	0.257
Shoulder	0.025	0.020-0.030	0.013	0.259

The success of the above work indicated that the thicker clad should present no problems. During the next period the end-cap welding program will be directed toward optimizing weld parameters for 0.013 in. walled fuel bearing tubes. Reproducibility runs will be made. Additional welds will be made, as required to provide fuel tubes for experimental programs.

The reference process will be established, and a final report of the program will be written.

I.6.5. FUEL BUNDLE ASSEMBLY

I.6.5.1. Fabrication Development. This investigation is being performed to develop methods for producing accurately spaced high-integrity seven-rod bundles for Pathfinder. Work during the last period included installation of a 3-ft long furnace for high-temperature brazing studies. Tee-joint samples were brazed to study effects of time and braze quantity. A fuel bearing assembly was brazed using swaged-compacted fuel rods. Work was initiated to braze mock-up test assemblies. Work on high frequency welding was continued.

Evaluation of tee-joint samples that were prepared using Nicrobraze 30, GE81, and Coast Metals 60 was completed. Results indicated no significant difference is any of the samples. A static corrosion test of samples of the three braze alloys is being conducted in 1000F steam.

A series of tee-joint samples were prepared to study interaction of braze quantity and braze time on joint integrity and microstructure. The primary objective was to produce brazements with a minimum of undiluted braze alloy in the interface and a minimum grain size in the base material. Preliminary runs have been made at 30 min. using braze quantities ranging from sufficient fill to three-times fill. Results thus far show all brazements to be excellent with no major difference in microstructure. Erosion, as expected, was more severe as braze quantity increased. Grain size in all samples was very large ranging from ASTM 1 to 3. The amount of undiluted braze alloy in the brazements varied within samples and seemed more a

function of braze quantity than time (Figures I.32 and I.33).

Components are now ready for brazing 5 min. at temperature. The shorter time at temperature should reduce base material grain size but would leave more undiluted braze material in the braze joint. Consequently, several samples will be annealed for 4 hr at 1750F to promote braze alloy diffusion.

Two 6-ft long seven-rod bundles and five 3-ft long bundles are being brazed. Fabrication will be performed by brazing 30 min at 2150F in dry hydrogen using Coast 60 alloy, Nicrobraze 30, and GE81. These samples will be used for studies of dimensional stability, physical properties, and metallurgical characteristics using the various materials.

A 3-ft long fuel assembly was prepared using swage-compacted fuel rods. Brazing was performed in vacuum at 2150F using Coast Metals 60 alloy. Due to a furnace malfunction, only half of the assembly was satisfactorily brazed. Evaluation indicated that dimensional quality was very poor. Braze integrity, based on external appearance, was excellent in the uniformly heated zone. An attempt will be made to repair this assembly by hanging it vertically in a vacuum retort and allowing the fuel rods to straighten themselves during a rebrazing cycle.

I.6.5.2. High-Frequency Welding Study. The new high-frequency welding equipment was installed. The equipment was used to make satisfactory welds of sheath thermocouple wire to 7/8-in dia. tubing (high-enrichment superheater fuel element), and spiral spacer wires to small diameter tubing.

Equipment. A general view of the welding equipment is given in Figure I.34. This equipment includes the following features.

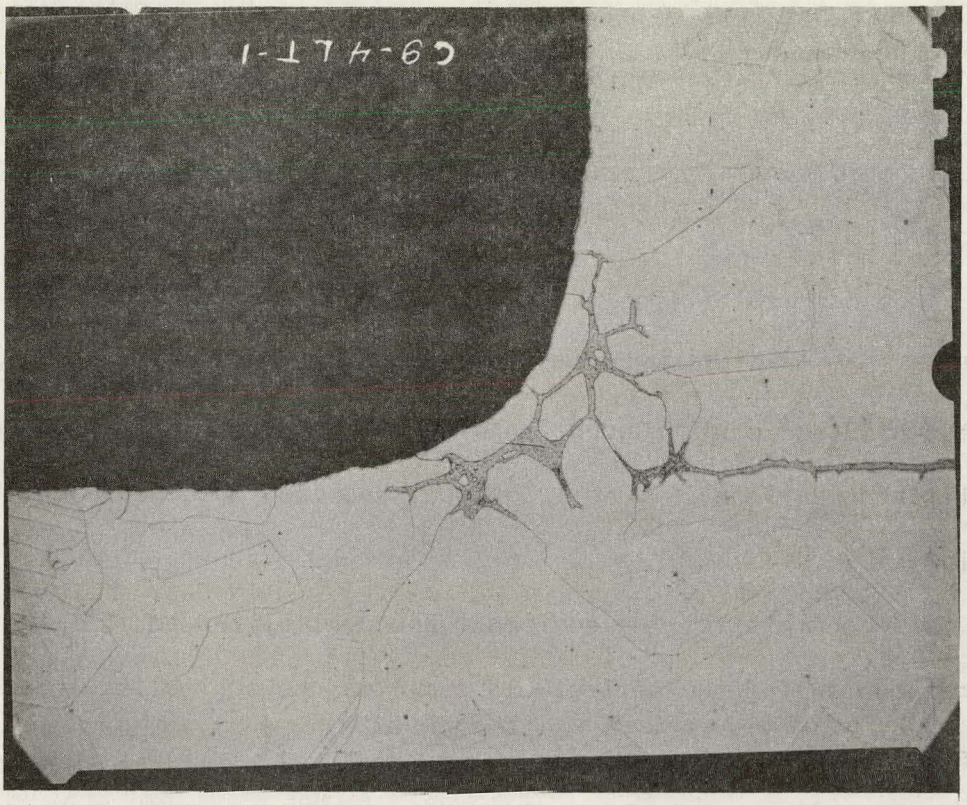

Figure 1.32 Typical tee-joint brazement using Coast Metal 60 at temperature for 30 minutes. Undissolved braze may be observed at the braze interface.

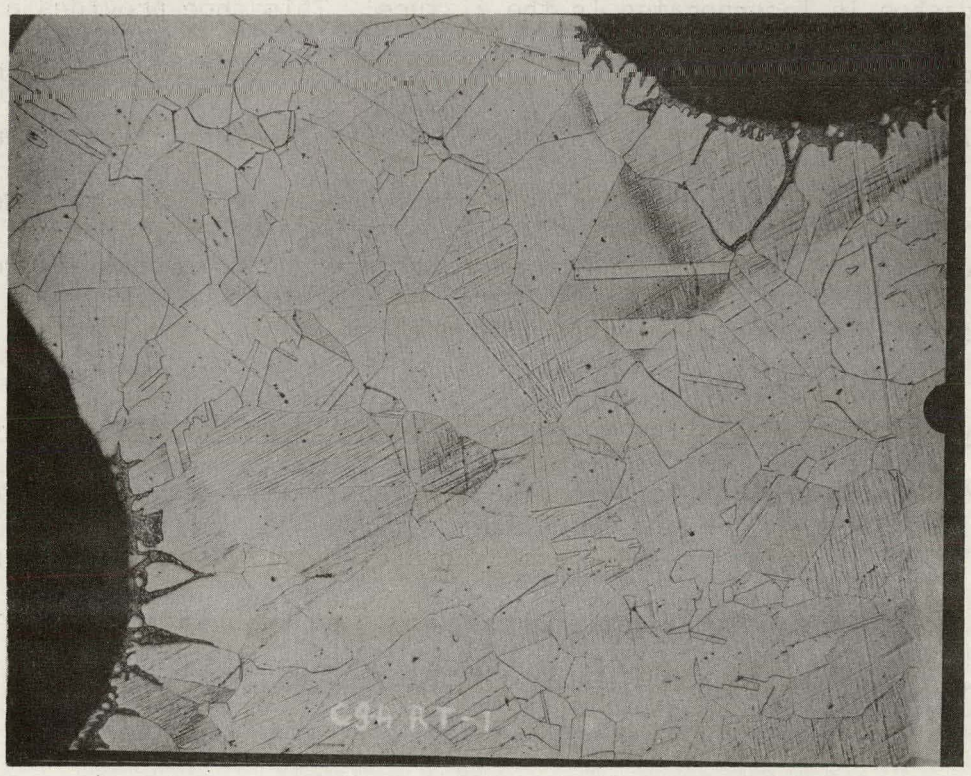

Figure 1.33 Typical tee-joint brazement using Coast Metal 60 at temperatue for 30 minutes. braze interface is clean with complete grain growth.

An autotransformer is used to provide close control of voltage with good reproducibility.

An electrical filter is included which reduces the 120-cps ripple voltage from the full-wave rectifier, from a factor of 48 per cent to a factor of 2 per cent. Reduction of these voltage fluctuations eliminated a stitching pattern (Figure 1.35) that had been obtained with the previous equipment.

All controls for the equipment are centralized so that the various operations during the entire weld cycle may be controlled independently or simultaneously.

The equipment includes a weld fixture (Figure 1.36) in which tubing from 0.200 to 1 in. O.D. and in lengths to 6 ft may be welded. The fixture provides accurate control of alignment and weld pressure. A fixed copper weld shoe is incorporated in the fixture. This shoe provides a more stable weld current because good conduction is less dependent on alignment and good wiping contact-surface as was the case with the wheel-type contact used on the previous equipment. Uneven contact between the wire and wheel had resulted in fused spots on the wire surface due to excessive current density. The shoe eliminated this problem.

Welds between Sheath Thermocouple Wire and Large-diameter Tubing. Experiments were run to determine the feasibility of welding straight 0.040 and 0.062 in. dia. sheath thermocouple wire to tubing ranging from 1/2 to 7/8 in. O.D. This weld if satisfactory would be used to instrument high-enrichment superheater fuel elements. A continuous weld is desired.

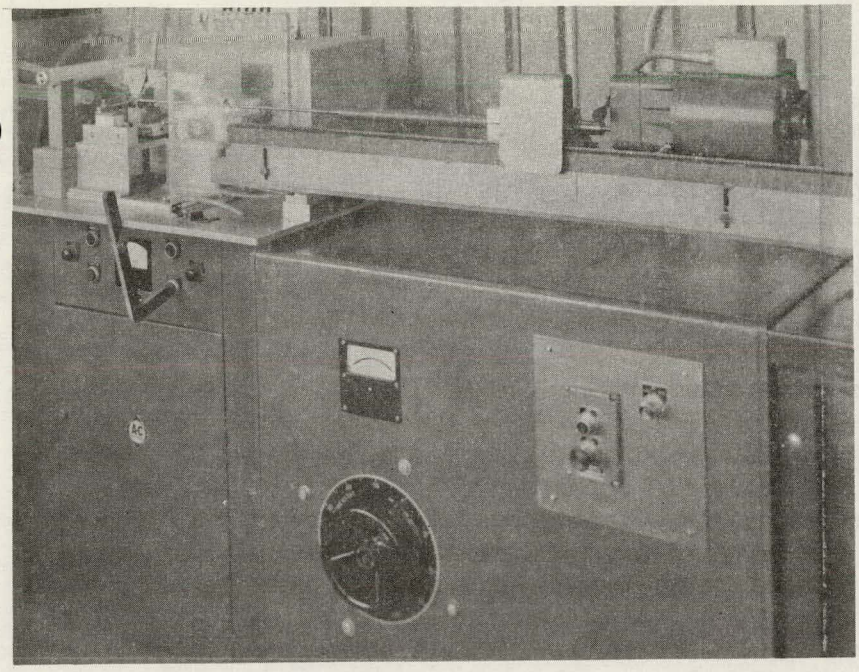

Figure I.34 General view of high-frequency welding equipment.

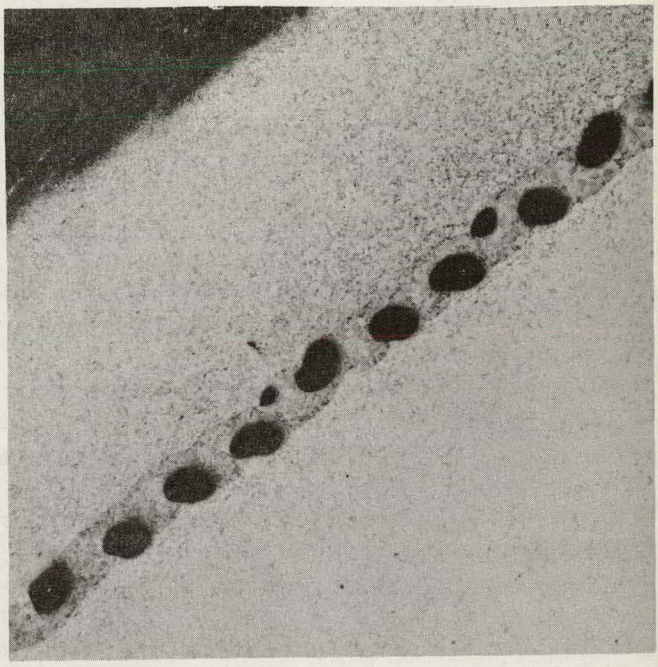

Figure I.35 Stitching pattern in welds made without adequate control of ripple voltage.

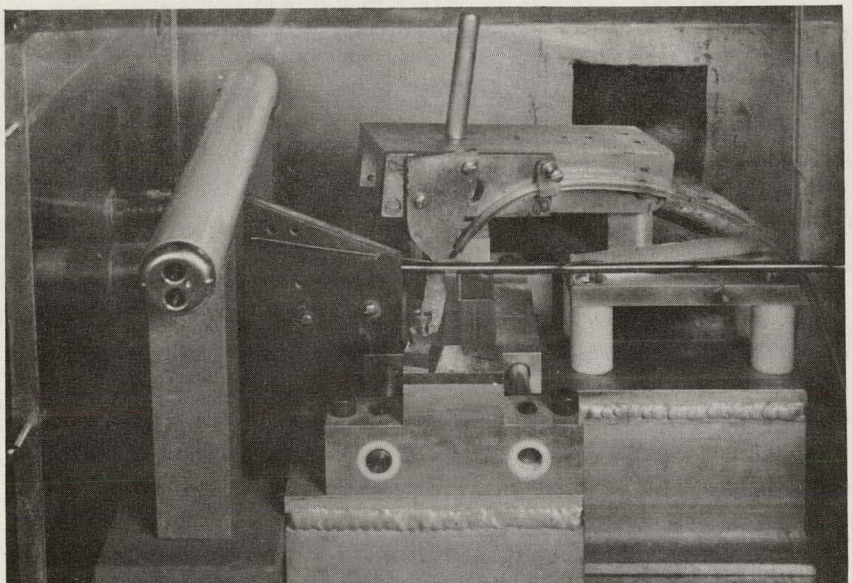

Figure I.36 Weld fixture for high frequency welding equipment.

Figure I.37 Unsymmetrical weld puddle obtained between thermocouple wire sheath and 0.035 in. tube wall.

The following welds were made:

a) 7/8 in. dia., 0.035 in. wall, 304 SS tubing to 0.040 in. dia. 316L SS sheath thermocouple wire.

b) 5/8-in. dia., 0.035 in. wall, 304 SS tubing to 0.062 in. dia. 316L SS sheath thermocouple wire.

The weld presents a problem with heat balance between the sheath and tube, which results in a strong but unsymmetrical weld puddle, as shown in Figure 1.37. The presence of a strong metallurgical bond is illustrated in Figure 1.38, which shows a transverse section of the weld and the ductile shear failure after the wire had been pulled away. Work is continuing to obtain a more symmetrical weld.

Welds between Spiral Spacer Wires and Small Diameter Tubing. Experiments were conducted to determine prime variables affecting penetration and distortion when welding spiral wire spacers to small diameter tubing. Variables investigated included wall thickness, wire lead, weld speed, and power output. Both empty and filled tubes were investigated.

Solid spacer wires 0.036 in. dia. were welded to the following 316L SS tubing.

a) 0.220 in. dia., 0.010 in. wall, empty and full.

b) 0.228 in. dia., 0.013 in. wall, empty.

c) 0.255 in. dia., 0.013 in. wall, empty.

Spiral leads of 3,6, and 12 in. were used.

Experiments are complete but evaluation is continuing. Preliminary evaluation indicates that good welds can be consistently made. Figure 1.39 shows a typical transverse section, and Figure 1.40 shows a section of tubing after the wire has been pulled off.

Preliminary evaluation also indicated that axial distortion increases as the wire lead increases. The spiral wire wrap results in very little tube bowing. Radial distortion is held within 0.0015 in. when welding a wire with a 3-in lead to 0.013 in wall empty tubing, and the radial distortion is less with filled tubing. Weld strength is satisfactory for reactor use.

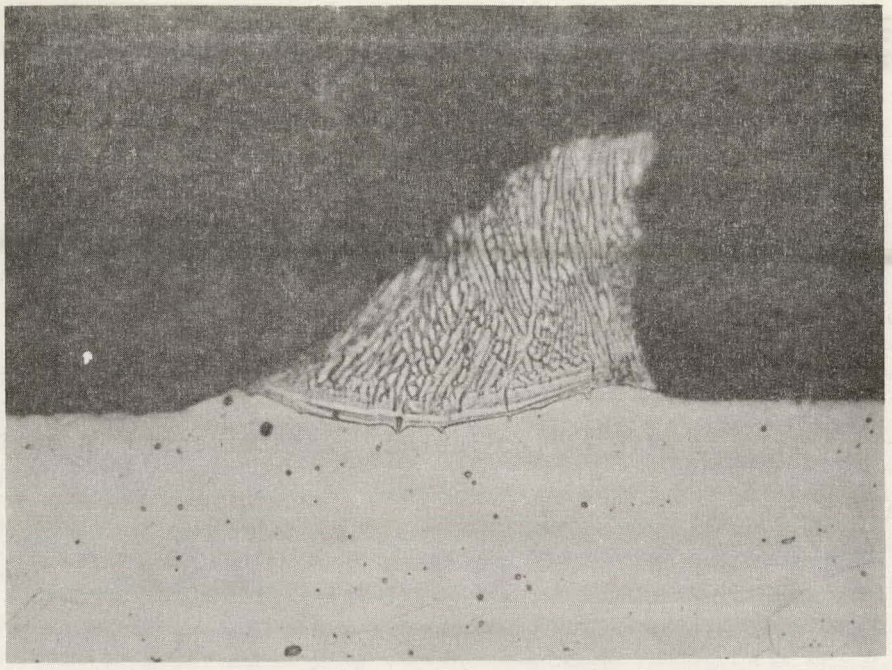

Figure 1.38 Transverse section of tube wall and weld after thermocouple sheath has been pulled away.

Figure 1.39 Transverse section of weld between spacer wire and tube wall.

1.40 Macrograph ot tube after acer wire has been removed.

2. REACTOR MECHANICAL STUDIES

THIS PAGE

WAS INTENTIONALLY

LEFT BLANK

2.4 CONTROL RODS, GUIDE TUBES, AND CONTROL ROD DRIVES

The objectives of this project are to fabricate and test a full-scale prototype control rod drive unit to experimentally determine the rate of movement, mechanical reliability, accuracy of position indicators, and scram operation under simulated Pathfinder operating conditions. Incident to these objectives are the development of a shaft-seal to minimize leakage of water or steam from the drive housing, fabrication and testing of a rack and pinion to operate in steam or water, fabrication and testing of a dashpot capable of repeated operation under the impact of the control rod under simulated reactor conditions, fabrication and testing of a submersible drive mechanism to drive the rack and pinion, and testing the mechanical operation to drive the rack and pinion, and testing the mechanical operation of the superheater control rod.

2.4.1 CONTROL ROD DRIVE

The prototype control rod drive was assembled with the H-1100-F heat-treated 17-4PH stainless steel rack and pinion. The pinion was not chrome-plated and the hardness of both pieces was 32 Rc. After 1100 cycles, the rotary shaft seal began leaking badly, the clutch began slipping, and, for the first time during tests of the prototype drive, the drive failed to scram.

The drive was dismantled. The rack and pinion were both worn badly, which caused jamming and the failure to scram. The pinion teeth were worn half through, and large burrs surrounded the contact area. The rack teeth were substantially rounded on the edges. The clutch slippage was due to overloading resulting from the worn gears. Chips caused the failure of the rotary shaft seal.

A test of a chrome-plated H-900-F heat-treated 17-4PH pinion (reference design) is planned. An identical pinion with chrome-plating that did not cover the teeth entirely was previously tested

with an inaccurately machined rack. The test had indicated that the pinion would have been satisfactory if chrome-plating had adhered satisfactorily and if the rack had been properly machined. The chrome-plating on the pinion that will be tested covers the teeth entirely, and should not peel.

The pinion will be tested with a spare 300-series stainless steel rack since a 17-4PH rack is not immediately available. The hardness of the 300-series rack is 22 Rc, which is sufficiently close to the hardness of the H-1100-F 17-4PH rack to provide a valid test of the pinion. If the pinion should fail in this test, it would definitely show that the chrome-plated pinion is not satisfactory.

A seal baffle was added to the drive to keep the chips and dirt out of the rotary shaft seal.

Transformer oil has been used in the drive. Since rust has formed on bearings, two oils with rust inhibitors were tested. With Mobil DTE 797 turbine oil, the motor speed decreased and the current increased. This oil was considered unsatisfactory for these reasons. With Mobil Velocite No. 6 oil, which has the same viscosity as the transformer oil, the drive operated satisfactorily.

3. NUCLEAR ANALYSIS

THIS PAGE

WAS INTENTIONALLY

LEFT BLANK

3.1 REACTOR PHYSICS (STATICS)

The objective of this project is to perform physics calculations such as computer programming and operation, and to determine the critical mass, neutron and gamma flux and power distribution, enrichment, coefficients of reactivity, control-rod effectiveness, and conversion ratio with respect to a Pathfinder core with an integral high-enrichment superheater region. An additional objective is to determine shielding requirements for the Pathfinder plant.

3.1.1 CONTROL ROD PROGRAM DURING REACTOR STARTUP

The effect of boiler control rod configurations on the superheater performance during reactor startup was discussed in the last technical progress report ACNP-62005. Superheater power fractions and the radial peak-to-average power ratio were shown for three specific control rod configurations. During the last quarter, further analysis was performed on control rod insertion and superheater performance during low power conditions.

Prior to the calculations for partially inserted control configurations, the expected critical control rod positions were generated as a function of reactor startup condition. This was done using the calculated excess reactivity values as a function of reactor condition shown in Table 3.1, the calculated control rod worths per control rod group for different core conditions shown in Table 3.2, and an integral control rod worth curve as a function of core height.

The excess reactivities were obtained from PDQ-RZ calculations normalized to include specific XY geometric effects. The control rod worths shown in Table 3.2 were obtained from XY calculations with control rods represented explicitly. Fast-group constants for the control rods were similar to those discussed in technical progress report ACNP-6012. A black boundary condition was used for the thermal group constants. The worth curve was obtained from the Allis-Chalmers Critical Experiment Facility for the full core Pathfinder mock up.

TABLE 3.1 REACTOR EXCESS REACTIVITY DURING STARTUP CONDITIONS

REACTOR CONDITION	ρ_{EX}
Cold, clean, superheater fully flooded	.1114
Cold, clean, superheater steam passages voided	.1160
Hot ($T_{mod} = T_{fuel} = 489F$), clean, superheater fully flooded	.0981
Hot ($T_{mod} = T_{fuel} = 489F$), clean, superheater steam passages voided	.1030
Hot, 20 per cent reactor power, clean, reactor pressure at 300 psia, exit void of 28 per cent by volume	.0834
Hot, 20 per cent reactor power, clean, reactor pressure at 600 psia, exit void of 18 per cent by volume	.0934
Hot, 20 per cent reactor power, equilibrium Xe, reactor Pressure at 600 psia, exit void of 18 per cent by volume	.0807
Hot, 50 per cent reactor power, clean, reactor pressure at 600 psia, exit void of 31 per cent by volume	.0795
Hot, 50 per cent reactor power, equilibrium Xe, reactor pressure at 600 psia, exit void of 31 per cent by volume	.0589
Full power, clean, exit void of 43 per cent by volume	.0690
Full power, equilibrium Xe, exit void of 43 per cent by volume	.0388
Full power, equilibrium Xe and Sm, exit void of 43 per cent by volume	.0314

TABLE 3.2 PATHFINDER CONTROL ROD WORTH FOR DIFFERENT CORE CONDITIONS

4 Superheater control rods---------- Group I

*4 Boiler control rods immediately adjacent to superheater core (#5, 8, 9, 12)---------- Group II

*4 Boiler control rods at superheater core corners (#4, 6, 11, 13)------ Group III

*8 Boiler control rods at outer edge of core (#1, 2, 3, 7, 10, 14, 15, 16)---------- Group IV

Control rod identification is given in ACNP-6117, Figure 3.1.

CORE CONDITION AND CONTROL CONFIGURATION	CONTROL ROD GROUP	WORTH Δk/k
Cold (68F) - CRG I, II, III, IV, Inserted	All control rods	.1430
Cold (68F) - CRG I, III, IV, Inserted	II	.0713
Cold (68F) - CRG I, II, III, Inserted	IV	.0671
Hot (T_{mod}= 489F), Unvoided - CRG I, II, III, IV, Inserted	All control rods	.1860
Hot (T_{mod}= 489F), Unvoided - CRG I, III, IV, Inserted	II	.0925
Hot (T_{mod}= 489F), Unvoided - CRG I, II, IV, Inserted	III	.1004
Hot (T_{mod}= 489F), Unvoided - CRG I, II, III, Inserted	IV	.0870
Hot (T_{mod}= 489F), Unvoided - CRG I, IV, Inserted	III	.0472
Hot (T_{mod}= 489F), Unvoided - CRG I, II, Inserted	III	.0644
Hot (T_{mod}= 489F), Unvoided - CRG II, IV, Inserted	I	.0172
Hot (T_{mod}= 489F), Unvoided - CRG III, IV, Inserted	I	.0181
Hot (T_{mod}= 489F), Unvoided - None Inserted	IV	.0325

* For the hot voided condition some control rod worths are given in ACNP-6117, Section 3.1.

The expected critical control rod configurations are shown in Table 3.3. These control rod configurations are described to 20 per cent of reactor power. The superheater control rods are inserted throughout to suppress the superheater power during the non-turbulent low-steam-flow, low-power condition.

To aid in determining which control rods or control rod groups should be withdrawn first, the effect of the control configuration on the radial peak-to-average power ratio and the superheater power fraction was investigated. Table 3.4 summarizes the results obtained for the lower core section in the hot non-voided core condition. Some calculations were also made for the upper core section. The peak-to-average radial power values for the superheater shown in the table represent results taken directly from the XY calculations.

The results shown in Table 3.4 are separated into two main groups; those control rod configurations with outer boiler control rods inserted, and those with outer rods withdrawn. For the latter cases, the superheater power fraction is lower, although the radial peak-to-average power ratio is somewhat higher. For the one case in which two of the Group-II control rods are withdrawn, the severe tilt developed across the core results in a high radial peak-to-average power factor. This indicates that the withdrawal of control rod groups would be the preferred mode of control rod motion for the two inner boiler control rod groups. Withdrawal of the outer boiler control rods has less of an effect on the radial peak-to-average power for the superheater. Consequently, these could be withdrawn individually or preferentially in paired groups.

In all of these calculations, the boiler core was void-free. For the voided condition, the radial peak-to-average factor would be reduced because of the better match between the boiler and superheater cores and also because

TABLE 3.3 CRITICAL CONTROL ROD CONFIGURATION AS A FUNCTION OF REACTOR OPERATING CONDITION

REACTOR CONDITION	CRITICAL CONTROL CONFIGURATION WITHDRAWING INNER BOILER RODS FIRST Calc. ρ_{EX}	CRITICAL CONTROL CONFIGURATION WITHDRAWING OUTER BOILER RODS FIRST Calc. ρ_{EX}
1. Cold, clean superheater flooded	I, III, IV fully inserted None withdrawn II partially withdrawn 28 in.	I, II, III fully inserted None withdrawn IV partially withdrawn 26 in.
2. Hot (T_m= 400F), superheater flooded	I, III, IV fully inserted None withdrawn II partially withdrawn 51 in.	I, II, III fully inserted None withdrawn IV partially withdrawn 58 in.
3. Hot (T_m= 400F), superheater steam passages voided	I, III, IV fully inserted None withdrawn II partially withdrawn 46 in.	I, II, III fully inserted None withdrawn IV partially withdrawn 51 in.
4. Hot (T_m= 489F), 20 per cent power N_O Xe, V_{EX} = 28 per cent, reactor pressure 300 psi	I, IV fully inserted II fully withdrawn III partially withdrawn 22 in.	I, II fully inserted IV fully withdrawn III partially withdrawn 21 in.
5. Hot (T_m= 489F), 20 per cent power N_O Xe, V_{EX} = 18 per cent, reactor pressure 600 psi	I, IV fully inserted II fully withdrawn III partially withdrawn 15 in.	I, II fully inserted IV fully withdrawn III partially withdrawn 17 in.

TABLE 3.4

EFFECT OF CONTROL ROD CONFIGURATION ON SUPERHEATER OPERATION (POWER FRACTION AND RADIAL PEAK/AVG POWER) DURING STARTUP (XENON FREE)

CONTROL CONFIGURATION	SUPERHEATER POWER FRACTION	RADIAL POWER PEAK/AVG
All control rods inserted	.1331	1.89
Control rod group I, II, IV, inserted	.0954	2.48
Control rod group II, IV, inserted	.1617	1.62
Control rod group I, III, IV, inserted	.1094	2.15
Control rod group III, IV, inserted	.1780	1.37
Control rod group I, IV, inserted	.0923	2.18
Control rod group I, II, III, inserted	.0696	2.18
Control rod group I, II, inserted	.0639	2.53
Control rod group I, III, and 2 of Group II	.0670	3.27

of the void redistribution resulting in power flattening. All of these calculations were performed for the Xe and Sm free condition.

Investigation of partially inserted control rod configurations was made using a nuclear model very similar to that described in the core burnup section of technical progress report ACNP-6117. The boiler core was divided into three annular regions, in which specific boiler control rods were located as a homogenized poison. The preservation of XY core power distribution and core reactivity was obtained by the proper selection of homogenized poison. Fast and thermal control absorptions were accounted for by fast and thermal values of homogenized poison. The adequacy of this representation was determined by comparing one-dimensional radial results to the two-dimensional XY results in which the control rods had been represented explicitly.

Using the radial model as described above, RZ-PDQ calculations were made for the following partially inserted control rod conditions:[2]

1. 20 per cent reactor power, 300 psi reactor pressure, 28 per cent exit voids, clean:

   Control rod groups 1 and 4 fully inserted
   Control rod group 2 fully withdrawn
   Control rod group 3 withdrawn 19 inches

2. Same reactor conditions as above,

   Control rod groups 1 and 4 fully inserted
   Control rod group 2 fully withdrawn
   Control rod group 3 withdrawn 30 inches

3. Same reactor conditions as above,

   Control rod groups 1 and 2 fully inserted
   Control rod group 4 fully withdrawn
   Control rod group 3 withdrawn 30 inches.

(2) Control rod groups are defined in Table 3.1.

The first two cases represent probable critical configurations if the outer boiler control rods were not withdrawn first, and the latter case, the configuration that would exist under the present program of control rod withdrawal. These cases were selected because they represent the probable partial control rod insertion configuration that would have the most adverse effect on superheater performance. Partial control rod insertion to two different core heights, problems 1 and 2, were performed to obtain information on the critical height which yields the maximum tilt in the axial power distribution. These problems also provided a separate evaluation for the integral control rod worth curve as a function of core height discussed earlier.

In Table 3.5 and Figures 3.1, 3.2, and 3.3, axial power distributions for the hottest superheater channel summarize the effect of the partial control rod insertion on the superheater performance. The distributions shown in Figures 3.1, 3.2, and 3.3 were obtained by synthesizing explicit XY distributions obtained for specific core slices with the overall RZ distribution. This technique is discussed in some detail in section 1.6.1 of technical progress report ACNP-6123. The average power in the superheater has been normalized to 1.0 in those figures. From these distributions and superheater power fractions, a thermal analysis is being performed on the superheater.

Further work on the effect of partial control rod insertions, both boiler and superheater, at higher power conditions on the superheater and boiler core performance will be done next quarter.

TABLE 3.5 EFFECT OF PARTIAL CONTROL ROD INSERTION ON REACTOR PERFORMANCE

(20 per cent power, 28 per cent exit void, 300 psi, clean)

REACTOR CONDITION AND CONTROL ROD CONFIGURATION Control Rod Position Group	AXIAL POWER DISTRIBUTION (Figure)	k_{eff}	SUPERHEATER POWER FRACTION	SYNTHESIZED OVERALL P/A POWER IN SUPERHEATER
I, IV inserted II withdrawn III withdrawn 20 in.	1	.992	.1283	2.99
I, IV inserted II withdrawn III withdrawn 30 in.	2	1.004	.1233	3.05
I, II inserted IV withdrawn III withdrawn 30 in.	3	1.004	.0872	4.29

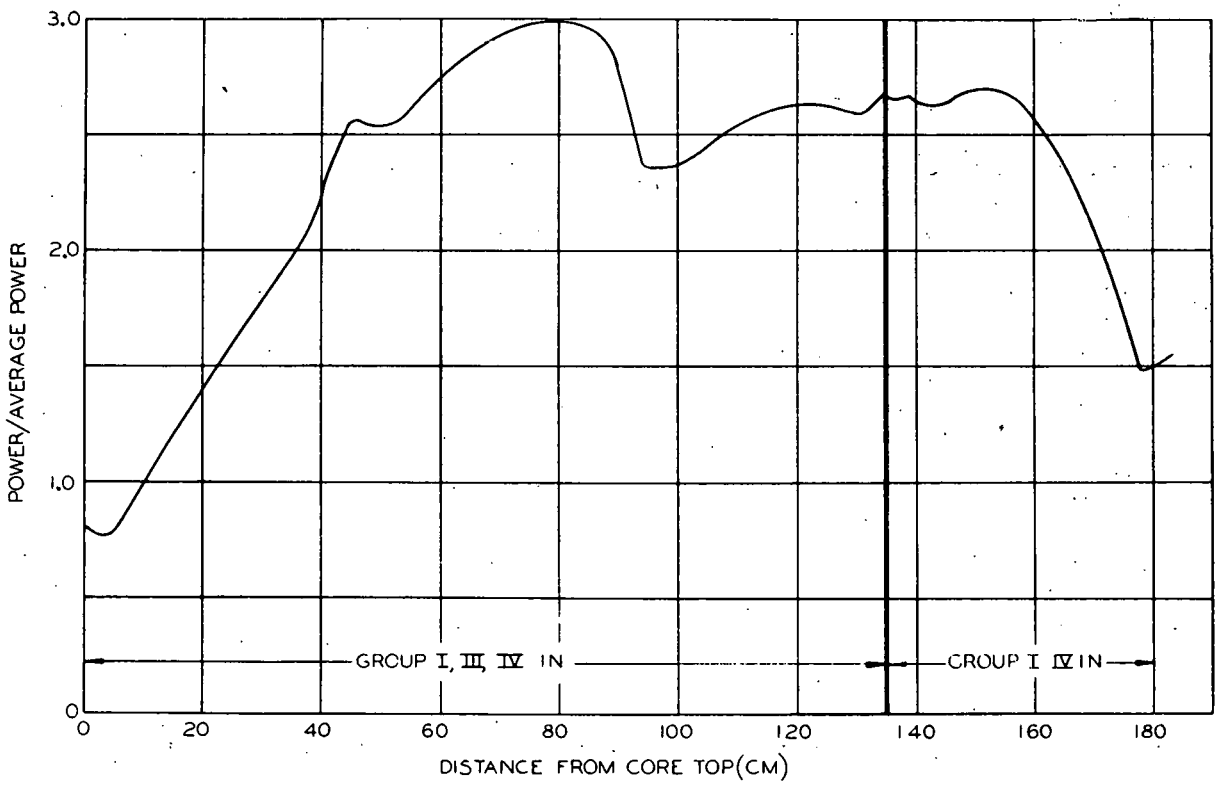

Figure 3.1 High-enrichment superheater hot-channel axial power distribution with Groups I and IV fully inserted and Group III withdrawn 20 in. (A-C Dwg 43-025-147)

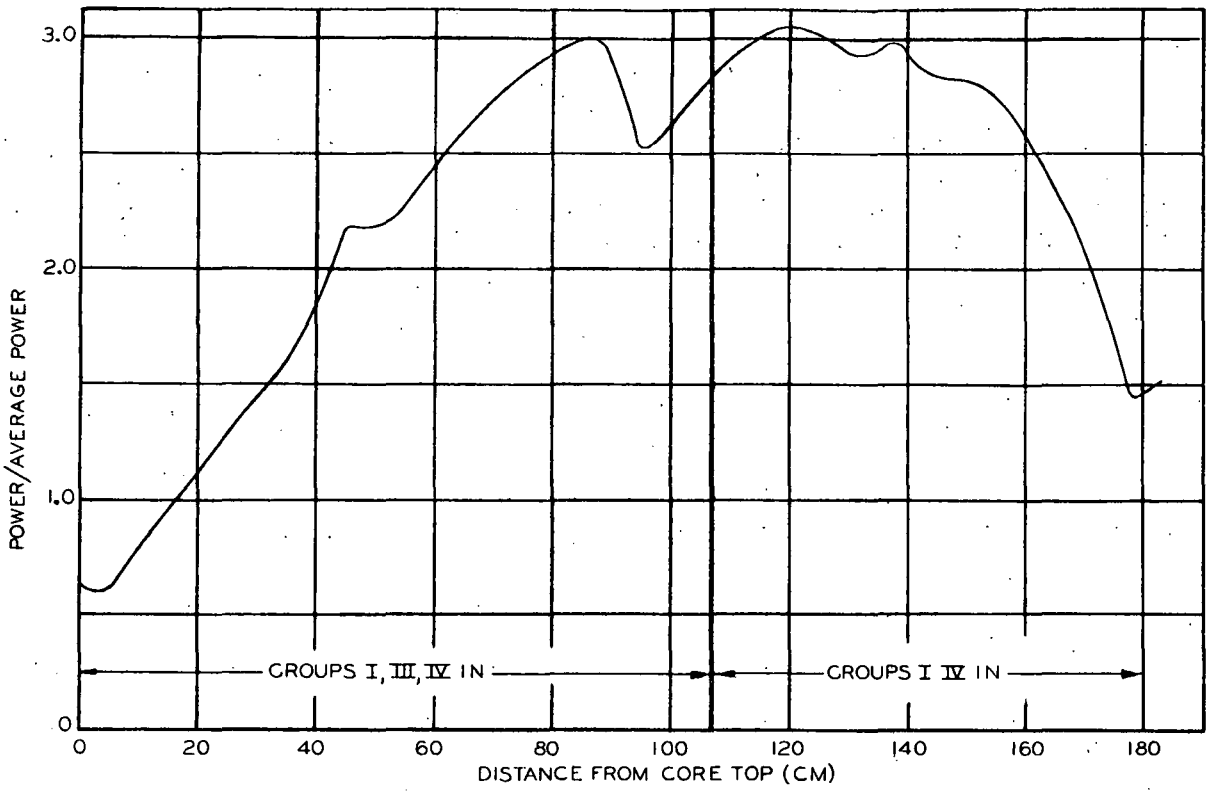

Figure 3.2 High-enrichment superheater hot-channel axial power distribution with Groups I and IV fully inserted and Group III withdrawn 30 in. (A-C Dwg 43-025-149)

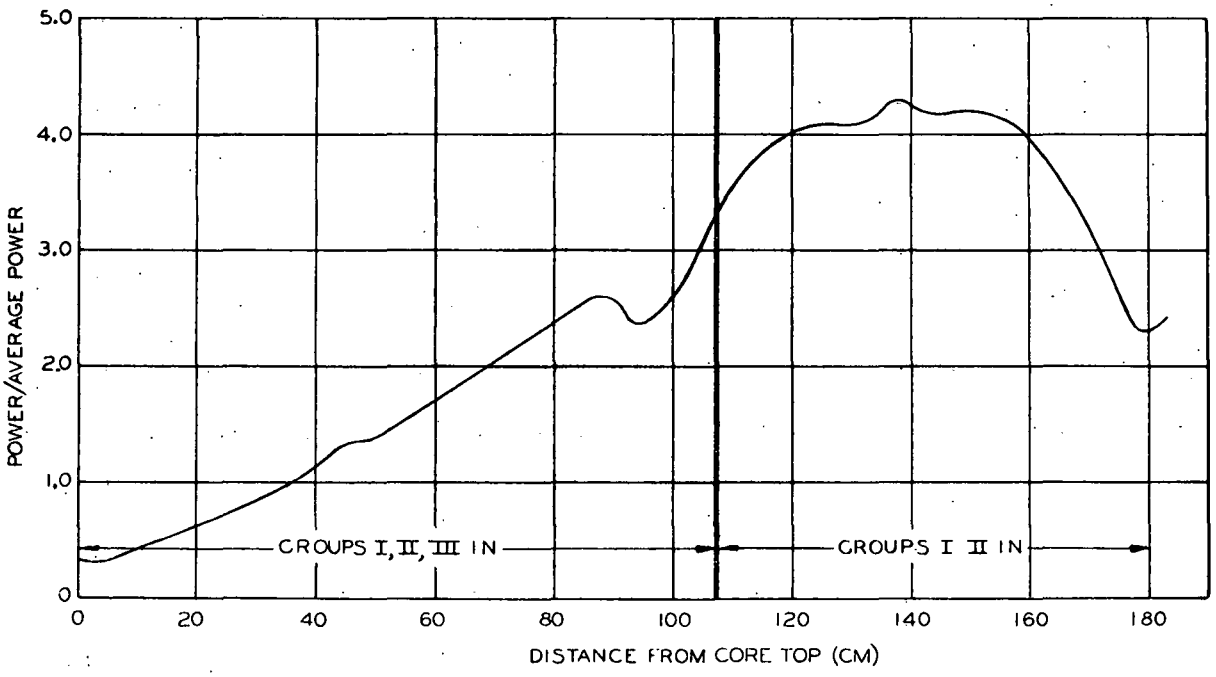

Figure 3.3 High-enrichment superheater hot-channel axial power distribution with Groups I and II fully inserted and Group III withdrawn 30 in. (A-C Dwg 43-025-150)

3.2 REACTOR AND SYSTEM DYNAMIC ANALYSIS

The objectives of this project are to perform reactor transient analysis under normal operation and after credible or hypothetical accidents involving equipment failure or reactor misoperation, as well as a system stability analysis using an analog simulator or digital computer.

3.2.1 MULTI-SECTION SUPERHEATER

More refined studies on the detailed multi-sectioned superheater have shown that the 10-section (axial) analog model yields hot-spot superheater fuel temperatures about 2 per cent lower than a lumped, single-section model, for a special stuck dump-valve accident.

Figure 3.4 shows maximum superheater fuel hot-spot temperature versus number of axial sections for this steam flow disturbance. On this figure the results are shown for 10-, 6-, 3-, 2-, and 1-section fuel models that received identical power and steam flow inputs. It can be seen that the lumped, one-section model is conservative in that it predicts higher temperatures than the 10-section model.

This curve and other data lead one to conclude that about 6-sections are sufficient to yield accurate axial spatial temperatures during a transient. The ART-04 results for a 10-section (digital) model agree very closely with the 10-section analog model for an identical steam flow disturbance.

Another, more severe transient, a step increase in power, showed that the one-section model yielded temperatures about 5 per cent lower than the 10-section analog model.

3.2.2 XENON INDUCED INSTABILITY

An analysis was undertaken to determine whether uneven xenon buildup in Pathfinder could cause oscillation of the flux shape, the total reactor power

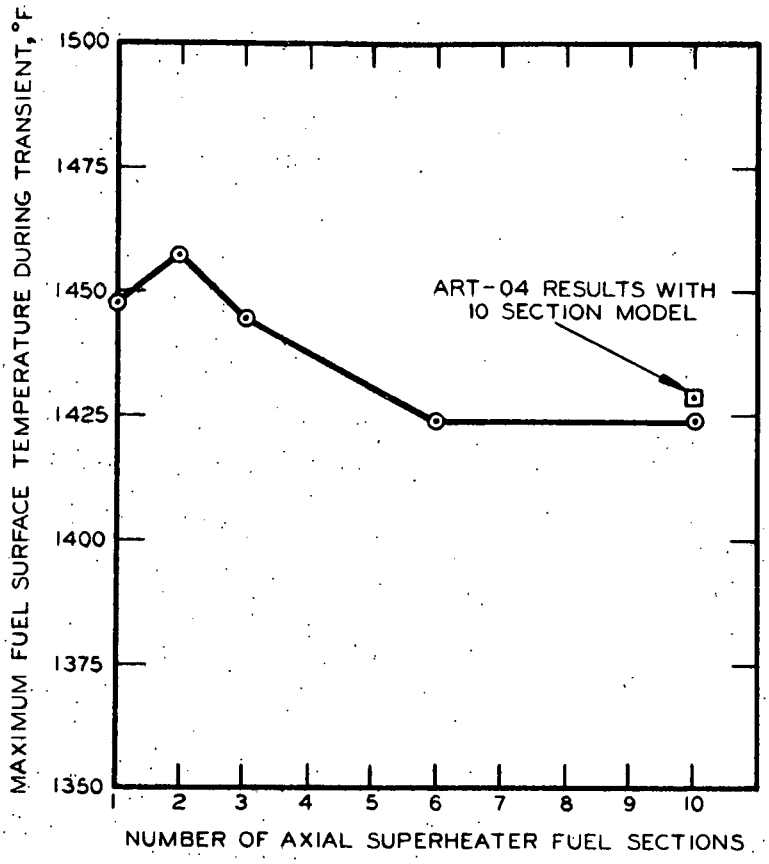

Figure 3.4 Multi-section superheater. Comparison of a number of axial sections for a special load dump accident. (A-C Dwg 43-025-175)

remaining constant. Included in the study was the effect of the power coefficient of reactivity on the oscillations. Using an analytical method previously proved [3] and a two-group, two-dimensional, two-region, analog model it was demonstrated that a core with Pathfinder characteristics (including adjacent superheater and boiler sections) would not be subject to xenon oscillations if it is less than about 11 ft in length and/or about 12 ft in diameter. Thus, the 6 X 6 ft Pathfinder core will not be subject to this phenomenom of flux shape oscillations.

(3) "Space- & Time-Dependent Flux Oscillations (and Instability) in Thermal Reactors Due to Nonuniform Formation and Depletion of Xenon", R. S. Wick, WAPD-TM-138.